Title: Calcium activation of cortical neurons by continuous electrical stimulation: Frequency-dependence, temporal fidelity and activation density

Nicholas J. Michelson[1,2], James R. Eles[1,3], Alberto L. Vazquez[1,3,4,5,6], Kip A Ludwig[7,8], Takashi DY Kozai[1,3,6,9,10*]

1. Department of Bioengineering, University of Pittsburgh, Pittsburgh, PA 15213, USA
2. Department of Psychiatry, University of British Columbia, Vancouver, BC V6T 1Z3, CA
3. Center for the Neural Basis of Cognition, University of Pittsburgh, Pittsburgh, PA 15213, USA
4. Department of Radiology, University of Pittsburgh, Pittsburgh, PA 15213, USA
5. Department of Neurobiology, University of Pittsburgh, Pittsburgh, PA 15213, USA
6. Center for Neuroscience, University of Pittsburgh, Pittsburgh, PA 15213, USA
7. Department of Biomedical Engineering, University of Wisconsin Madison
8. Department of Neurological Surgery, University of Wisconsin Madison
9. McGowan Institute of Regenerative Medicine, University of Pittsburgh, Pittsburgh, PA 15213, USA
10. NeuroTech Center, University of Pittsburgh Brain Institute, Pittsburgh, PA 15213, USA

Abbreviated title (50 characters): Spatiotemporal activation by microstimulation

Key words: microstimulation, bioelectric medicine, brain-computer interface, deep brain stimulation, neuroprosthetics

Support: NIH NINDS R01NS094396, R01NS094404, R01NS062019, R01NS089688, and R21 NS108098

***Correspondence:** 208 Center for Biotechnology and Bioengineering; 300 Technology Dr. Pittsburgh, PA 15219 tdk18@pitt.edu

Abstract
Electrical stimulation of the brain has become a mainstay of fundamental neuroscience research and an increasingly prevalent clinical therapy. Despite decades of use in basic neuroscience research and the growing prevalence of neuromodulation therapies, gaps in knowledge regarding activation or inactivation of neural elements over time have limited its ability to adequately interpret evoked downstream responses or fine-tune stimulation parameters to focus on desired responses. In this work, *in vivo* two-photon microscopy was used to image neuronal calcium activity in layer 2/3 neurons of somatosensory cortex (S1) in male C57BL/6J-Tg(Thy1-GCaMP6s)GP4.3Dkim/J mice during 30 s of continuous electrical stimulation at varying frequencies. We show frequency-dependent differences in spatial and temporal somatic responses during continuous stimulation . Our results elucidate conflicting results from prior studies reporting either dense spherical activation of somas biased towards those near the electrode, or sparse activation of somas at a distance via axons near the electrode. These findings indicate that the neural element specific temporal response local to the stimulating electrode changes as a function of applied charge density and frequency. These temporal responses need to be considered to properly interpret downstream circuit responses or determining mechanisms of action in basic science experiments or clinical therapeutic applications.

Significance Statement

Microstimulation of small populations of neurons has the potential to ameliorate symptoms associated with several neurological disorders. However, the specific mechanisms by which microstimulation elicits therapeutic responses are unclear. This work examines the effects of continuous microstimulation on the local population of neurons surrounding the implanted electrode. Stimulation was found to elicit spatiotemporal neuronal responses in a frequency dependent manner. These findings suggest that stimulation frequency may be an important consideration for applications in research or therapy. Further research aimed at understanding these neuronal activation properties may provide insight into the mechanistic mode of action of continuous microstimulation.

Introduction

Understanding the complexity of the nervous systems requires the ability to readout detailed measurements from controlled inputs (Adrian, 1928; Adrian & Bronk, 1928; Adrian & Matthews, 1928; Sherrington, 1910). While many new techniques and technologies are emerging, electrical stimulation remains one of the oldest and most widely used methods for directly interfacing and driving the nervous system(Du Bois-Reymond, 1884; Fritsch & Hitzig, 1870; Galvani, 1791; Galvani & Aldini, 1792; Volta, 1800). The ability to directly apply electrical potentials to individual nerves has helped identify biophysical properties of nerves and neurons(Eccles, 1953; Hodgkin & Huxley, 1952), and has been crucial in understanding the organization of the brain (Penfield & Boldrey, 1937; Spiegel, Wycis, Marks, & Lee, 1947). These studies also opened the door to electrical stimulation approaches for therapeutic applications (Delgado, Hamlin, & Chapman, 1952). Electrical stimulation has been used for hearing(Djourno, Eyries, & Vallancien, 1957; Doyle Jr, Doyle, Turnbull, Abbey, & House, 1963; L. R. House, 1987; W. F. House, 1976), vision (W. Dobelle & Mladejovsky, 1974; W. H. Dobelle, Mladejovsky, & Girvin, 1974), and somatosensory restoration (Cushing, 1909; Flesher et al., 2016) as well as for treating movement disorders (Alberts et al., 1965; Hassler, Riechert, Mundinger, Umbach, & Ganglberger, 1960; Sem-Jacobsen, 1966; Sem□Jacobsen, 1965), chronic pain (Gol, 1967; Mayer & Liebeskind, 1974; Richardson & Akil, 1977a, 1977b), and epilepsy (Marcos et al., 2000; Robert et al., 2010). More recently there has been an expansion of neuromodulation clinical trials, with over 1000 clinical trials registered on clinicaltrials.gov utilizing implanted or non-invasive electrodes to activate or inactivate nervous tissue. Some of these application include treatment of diverse conditions such as Tourette's syndrome, obsessive compulsive disorder, depression, Alzheimer's disease, and stroke. These clinical applications further motivate the development of improved chronically implanted electrical stimulation devices (LifeScienceAlley, 2015).

Despite its growing prevalence in scientific and clinical research, there is limited understanding of how electrical stimulation directly interacts with the complex milieu of neuronal and non-neuronal cells in the brain near the electrode. In acute mapping experiments of peripheral nerve fibers, short pulses of electrical stimulation were hypothesized to activate a small sphere of fibers in the local vicinity of the electrode (Ranck,

1975; Rattay, 1999; Stoney Jr, Thompson, & Asanuma, 1968; Tehovnik, 1996), with increases in amplitude increasing the volume of the sphere activated. When applying cathodic leading stimulation waveforms, increasing the amplitude could also cause a small zone of inactivation near the electrode tip, due to the generation of virtual anodes more distant from the tip, ultimately hyperpolarizing axons and preventing the propagation of any action potentials (Ranck, 1975). In contrast, recent experiments utilizing 2-photon calcium imaging to visualize the activation of neural elements in cortex near the electrode site found that electrical stimulation activated a sparse population of neuronal somas distant from the electrode site (Histed, Bonin, & Reid, 2009). These experiments demonstrated that electrical stimulation activates a much smaller volume of neural processes around the electrode tip, which in turn activate the connected soma (Histed et al., 2009).

Although changes in pulse amplitude are widely understood to alter the area of activation within the vicinity of the electrode, the extent to which different stimulation frequencies and pulse train durations affect local neuronal responses remains less explored. In this study, *in vivo* multiphoton calcium imaging of GCaMP6 transgenic mice was employed to elucidate how neuronal elements near an implanted electrode respond to different electrical stimulation frequencies over the course of a longer pulse train. Transgenic GCaMP6 mice allow for the probing of neuronal activity with high fidelity in a large proportion of cortical excitatory neurons without the need for exogenous calcium chelators. Stimulation was carried out at different frequencies using a 30 second burst of cathodic leading symmetric pulses, with a 50 µs pulse width/phase and pulse amplitudes within the established Shannon safety limits to avoid tissue damage (Shannon criteria of *k* between 0.12 and 1.3, 2.5 nC per phase). Based on the results of Histed et al (Histed et al., 2009) and Stoney et al (Stoney Jr et al., 1968), we hypothesized that both sparse and distributed activation would occur in cortex with continuous electrical stimulation at sufficient charge/phase. Our results support this hypothesis, but also demonstrate that different neural elements (neurites, soma) in the vicinity of the electrode differ in their responses as a function of time (stimulation onset, during, and after stimulation), space, and stimulation frequency. These data show a complex response profile near the electrode to electrical stimulation that may have significant implications for the design of electrical neuromodulation experiments and therapies. Hence, it is not surprising that different studies utilizing different charge/phase, frequencies, and time points yield conflicting results.

Methods

Surgery and electrode implantation

Transgenic mice C57BL/6J-Tg(Thy1 GCaMP6s)GP4.3Dkim/J (n=5, male, 22–28 g; IMSR Cat# JAX:024275, RRID:IMSR_JAX:024275) were used in this experiment. All surgical interventions were performed on adult mice (>4 weeks of age) that were housed in social housing with 12h light / 12h dark cycles and free access to food and water until acute experimentation. All animals were induced with an anesthetic mixture consisting of 75 mg/kg ketamine and 7 mg/kg xylazine administered intraperitoneally and updated with 40 mg/kg as needed. Rectangular craniotomies (~4 mm per side) were made over each somatosensory cortex and electrodes were implanted at a 30º angle as previously described (Eles et al., 2017; T. D. Kozai, Vazquez, Weaver, Kim, & Cui, 2012; Takashi D. Y. Kozai, Eles, Vazquez, & Cui, 2016; Takashi D Y Kozai, Jaquins-gerstl, Vazquez, Michael, & Cui, 2016; Michelson et al., 2018; S. M. Wellman & Kozai, 2018). Electrical stimulation was conducted through a single-shank 16-channel Michigan style functional silicon probes with 703 μm^2 electrode sites (NeuroNexus Technologies, Ann Arbor, MI). In order to prevent mechanical strain-related Ca activity caused by microelectrode insertion (Eles, Kozai, Vazquez, & Cui, 2018) from influencing stimulation evoked GCaMP activity, the tissue was allowed to rest 20 minutes after insertion prior to stimulation experiments. All experimental protocols were approved by the University of Pittsburgh, Division of Laboratory Animal Resources and Institutional Animal Care and Use Committee in accordance with the standards for humane animal care as set by the Animal Welfare Act and the National Institutes of Health Guide for the Care and Use of Laboratory Animals.

Two-photon Imaging

A two-photon laser scanning microscope (Bruker, Madison, WI) and an OPO laser (Insight DS+; Spectra-Physics, Menlo Park, CA) tuned to a wavelength of 920 nm at 15 mW was used for the entirety of this study. A16X 0.8 numerical aperture water immersion objective lens (Nikon Instruments, Melville, NY) was selected for its 3 mm working distance. Imaging was carried out over a 407 x 407 µm ROI, collected with a 512 x 512 pixel matrix. Before imaging sessions, animals were injected IP with 0.1 ml of 1mg/ml SR101 for visualization of blood vessels and electrode contacts. Imaging plane was positioned 10 µm above the electrode site, 120-150

µm below the surface of the brain. In order to image neural dynamic during electrical stimulation, time series images were recorded at 30 Hz and 2x optical zoom. The imaging plane for time series was set right over the electrode contact, so that the stimulating contact is visible during imaging session.

Electrical stimulation

Concurrent stimulation and imaging typically commenced 20 minutes after electrode implantation to allow time for displaced tissue to settle. An A-M Systems 2100, single channel Isolated Pulse Stimulator (A-M Systems, Sequim, WA) or TDT IZ2 stimulator on an RZ5D system (Tucker-Davis Technologies, Alachua, FL) were used to apply current controlled cathodic leading biphasic symmetric (50 µs each phase) electrical microsimulation at 50µA and frequencies of 10, 30, 50, 75, 90, 130 and 250 Hz. However, in one animal, the impedance of the stimulated site was an order of magnitude lower than that listed by the manufacturer, suggesting minor insulation failure at the electrode/insulation interface, as noted in previously (Prasad et al., 2014). This has the net effect of slightly increasing the electrode interface area, requiring greater current to achieve the same effective charge density seen in other animals. In this animal, 100 µA stimulation current was necessary to drive GCaMP activity. Amplitude of stimulation was selected based on minimum current required to evoke activation during two photon live scanning. Charge/phase, charge density/phase and k values were calculated based on the Shannon's equation (Shannon, 1992). The *k* value used during stimulation was between -0.12 and 1.3, well within safety limits to avoid tissue damage. After initial collection of resting state activity for 2min, concurrent imaging and stimulation trials were acquired for 2 min at each frequency, which included 30 s of pre-stimulation baseline, 30s of stimulation and 60s of post-stimulation baseline. An additional 3 minutes was required between each trial to store the data after data collection. The two-photon microscope was synchronized to the stimulator via transistor-transistor logic (TTL) and 30 s stimulation was carried out after a 30 s delay from the start of the time series. Stimulation was carried out in increasing frequency and were not repeated in the same animal. However, in two animals, 10 Hz stimulation was repeated at the end to determine if earlier microstimulation trials change the neuronal response properties for subsequent trials. The second 10 Hz stimulation data showed similar activation patterns to the first 10 Hz stimulation data.

Data analysis

Identification of activated neurons

The acquired time series images were converted to a single tiff image file using ImageJ (NIH). The tiff image was then analyzed using a custom MATLAB script (MATLAB, RRID:SCR_001622). Non-overlapping elliptical regions of interest (ROIs) were manually drawn around neurons to fully encompass their somas, which were identified by their morphology as bright rings of fluorescence (Fig 1b,d). ROIs were obtained using the CROIEditor MATLAB script, written by Jonas Reber (https://www.mathworks.com/matlabcentral/fileexchange/31388-multi-roi-mask-editor-class). Fluorescence intensity time-courses for each neuron were generated by averaging all pixels within a cell's ROI. Baseline fluorescence intensity (F_0) was calculated as the average signal during the 30-second pre-stimulation interval, and each time-course was then converted to changes in fluorescence ($\Delta F/F_0$). To identify activated neurons, each neuron's $\Delta F/F_0$ signal during stimulation was compared with their pre-stimulation $\Delta F/F_0$ signal. A fluorescence threshold of the mean pre-stimulation signal + three standard deviations (SD) was then established, such that neurons which showed $\Delta F/F_0$ changes that exceeded the threshold during stimulation were considered to be activated by the electrical stimulation. While it is possible that the threshold selection might not have identified all active cells, GCaMP6s is very sensitive to neuronal activity even for single action potentials (>30% $\Delta F/F$ reported) (Chen et al., 2013). Our criteria was robust for detection of low levels of activity even in the presence of small, unwanted signal changes due to motion or photomultiplier tube (PMT) dark current. The spatial locations and the activation properties of these neurons were then quantified for further analysis.

Neuropil Activation

Neuropil intensity was quantified by averaging the intensity level of a 10 x 25 µm region that did not contain neuronal somas. For each frequency, the neuropil was measured in the following distances from the edge of the electrode; 10-20, 30-40, 50-60, 100-110, 150-160, and 245-255 µm. Similarly, representative neuronal somas were selected at 15 and 115 µm from the electrode. F/F_0 of GCaMP intensities were computed where F_0 was the average GCaMP intensity of the 30 s pre-stimulus period.

Temporal activation pattern

Somas were classified as onset-responsive if they were activated during the first 0-2 seconds of the 30 second pulse train and ceased activation before the final 2 seconds of the pulse train (28-30 s). Somas were classified as steady-state-responsive neurons if they were active during 28-30 s post-stimulation onset. Duration of activity was calculated for each neuron by considering all time-points during stimulation which exceeded the intensity threshold. To examine the temporal characteristics of activated neurons in local vs distant or dense vs sparse groups, a weighted response time was estimated for each neuron. The 'Activation Time' was calculated as the time for which the cumulative ΔF/F sum reached 50% of the total ΔF/F sum over the 30s stimulation period. This expression describes the time it takes to cover half of the response energy. For example, a soma that reaches peak intensity at 0 seconds into the pulse train and maintains the exact same ΔF/F for all 30 s would have an 'Activation Time' of 15 s. Similarly, a soma that maintains a peak ΔF/F from 0 s to 5 s, but then falls to 20% of peak ΔF/F from 5 s to 30 s would have an 'Activation Time' of 5 s.

Spatial activation pattern

The spatial relationship between stimulation frequency and activity was determined by measuring the distance from the center of each active neuron to the nearest edge of the stimulating electrode site. The location of the center of the stimulating electrode site was visually identified from the same image series that was used to identify activated neurons and was confirmed with a high-resolution image taken immediately before the trial. The distances from the nearest edge of the stimulating electrode site to each activated neuron during the stimulation period were estimated for all animals and stimulation frequencies. The mean distance + 1SD was then calculated for each stimulation frequency and animal. Because the distance of onset and steady state activated neurons were considered for these calculations, distance thresholds remained fairly consistent across stimulation frequencies within animals. Therefore, the stimulation frequency with the minimum mean + 1SD for each animal was chosen to represent a distance threshold (139.7±18.8 µm for n=5), whereby cells in this region were considered local neurons, while those beyond the distance threshold were considered distant neurons.

Activation density

Density was examined as an independent measure by creating concentric circular bins, with an increasing radius of 20 µm drawn around the center of the electrode site. The number of fully encompassed, activated neurons within the area defined by each bin were counted from 0 to 30 s post stimulation onset, and then divided by the total area encompassed by that bin. Activated neurons were separated into dense or sparse populations, by establishing a threshold of mean density + 1 SD. To compare high and low-density activation patterns across stimulation frequencies, density thresholds were established for all stimulation frequencies, and the lowest mean density threshold was applied to all trials.

Statistical analysis

All data in boxplots show the sample median (eyes), 25th and 75th percentiles (top and bottom edges of box), 1.5 times the interquartile range (whiskers), and outliers (individual dots). To assess significance between stimulation frequencies, a repeated measures two-way ANOVA was performed (SPSS, RRID:SCR_002865), followed by post-hoc two-sample unequal variance t-test with a Bonferroni correction.

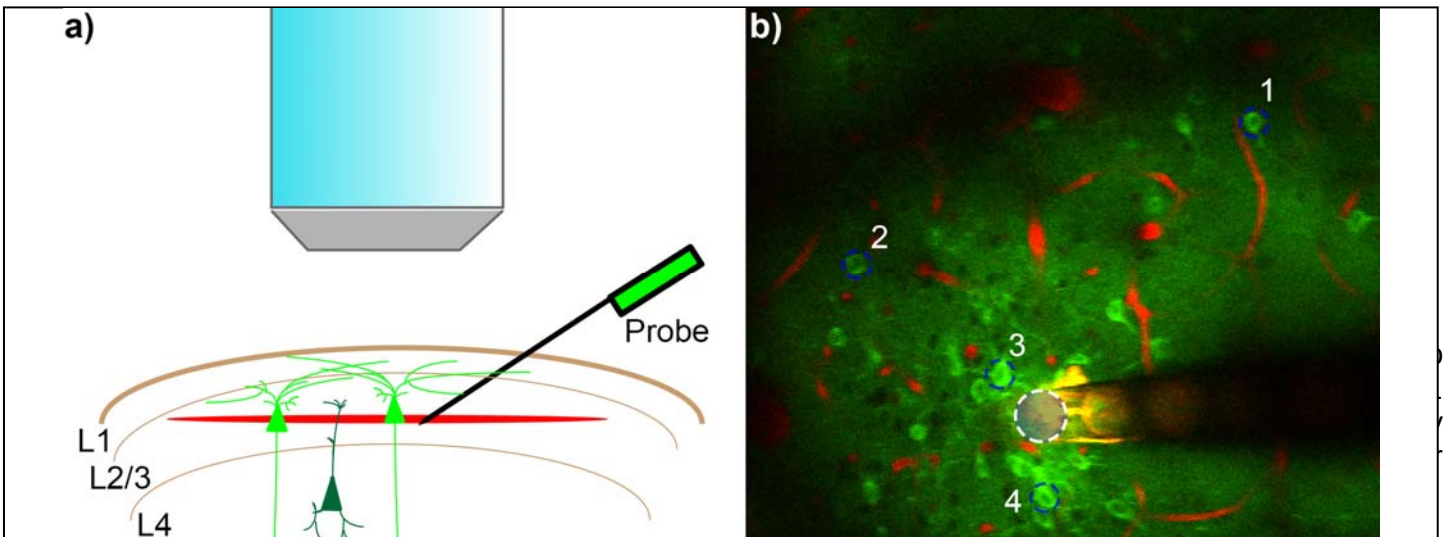

calcium indicators that largely reflect action potential firing (Chen et al., 2013; Dana et al., 2014; Greenberg, Houweling, & Kerr, 2008; Kerr & Denk, 2008; Sato, Gray, Mainen, & Svoboda, 2007; Smetters, Majewska, & Yuste, 1999). Because quiescent neurons have low GCaMP fluorescence, capillary visualization using 0.1 mg of sulforhodamin101 (SR101) was used to ensure the location of the electrode and visibility in the tissue with low laser power (< 20 mW), as previously described (Fig 1b) (Eles et al., 2017; T. D. Kozai et al., 2012; Takashi D. Y. Kozai et al., 2016; Takashi D Y Kozai et al., 2016; T. D. Y. Kozai et al., 2010; Michelson et al., 2018; S. M. Wellman & Kozai, 2018). Although GCaMP6 is more sensitive compared to other calcium indicators, such as Oregon green BAPTA, it has a longer decay constant that did not impair detection of activity(Chen et al., 2013). Evoked fluorescence traces show considerable variability in the intracellular calcium response to continuous stimulation (Fig 1c). Due to the binding constant, brightness, detector saturation, and temporal imaging resolution, it is not possible to quantify the calcium transients. The mouse line used in this study (GP4.3Dkim/J) has relatively high expression levels of GCaMP in layer II/III neurons (Dana et al., 2014), which was corroborated in a separate study, where this mouse line was imaged during a cortical spreading depression (Fig. 1d). The results demonstrate that sparse GCaMP activation noted during electrical stimulation is not due to sparse GCaMP expression in the genetic line.

The laminar probes were inserted with the electrode sites facing up and the imaging plane positioned approximately 10-15 µm above the electrode site in order to capture the neurons just above the stimulation site. The position of the imaging plane was confirmed through anatomical Z-stacks taken prior to the experiment. Co-registration of vasculature features outline of the implanted probe, and the electrode sites and traces were used to ensure that the imaging plane was just above the electrode site throughout the experiment. Electrical stimulation parameters matched previously employed protocols for neuroprosthetics and neuromodulation applications (De Balthasar et al., 2003; Kent & Grill, 2012; Kim et al., 2015; Shepherd & Javel, 1999; Wu, Levy, Ashby, Tasker, & Dostrovsky, 2001). Stimulation pulses were cathodic leading biphasic symmetric waveforms with pulse widths of 50 µs/phase (Lilly, Hughes, Alvord, & Galkin, 1955). Stimulation was performed for 30 s at a charge density and charge per phase below the Shannon safety limit for planar iridium electrode sites with 703 μm^2 surface area (Shannon, 1992) (< 3nC/phase) (Cogan, Ludwig, Welle, & Takmakov, 2016; D. B. McCreery, Yuen, Agnew, & Bullara, 1994). In general, stimulation was delivered at 50 µA and 50 µs, which has been previously shown to be just above the sensitivity threshold (Kim et al., 2015). The stimulation frequency was varied over different trials (Fig. 2-3; 10, 30, 50, 75, 90, 130, 250 Hz). As expected from previous reports (Histed et al., 2009), electrical stimulation led to sparse, distributed activation patterns (Fig. 2). Frequencies of 50 Hz and 130 Hz were selected as they are the frequencies at which the Shannon/McCreery safety curve was developed and the average optimal therapeutic frequency for deep brain stimulation (DBS) in Parkinson's Disease patients, respectively (Cogan et al., 2016; Shannon, 1992). These frequencies are compared to 10 Hz stimulation (Fig. 2).

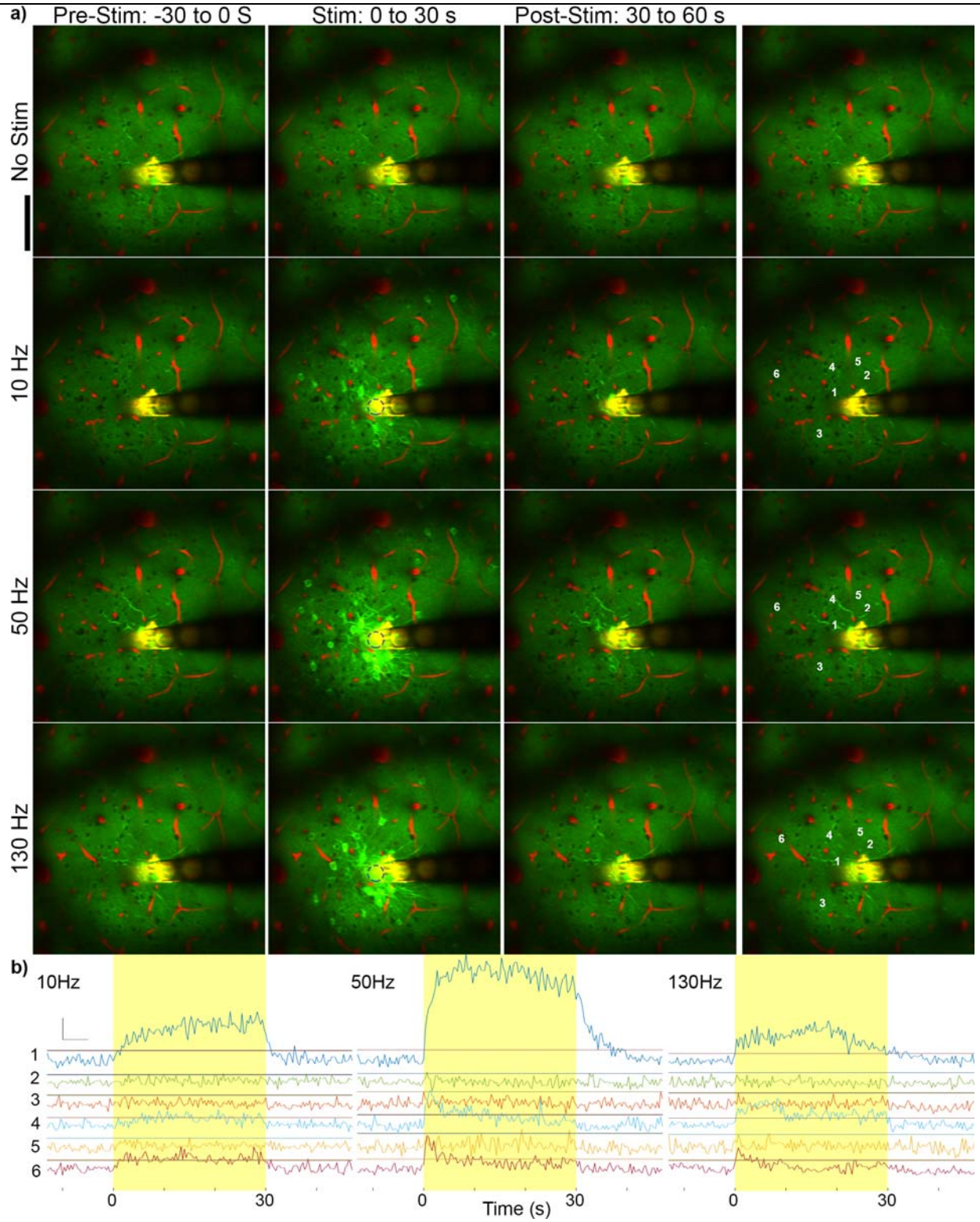

Figure 2: Stimulation frequency influences GCaMP activation pattern. a) Mean GCaMP imaging of 30 s prior to stimulation (left), during stimulation (middle), and post-stimulation (right) at no stimulation, 10 Hz, 50 Hz, and 130 Hz. Green indicates GCaMP labelled neurons and red indicates vasculature. The electrode sites and traces reflect fluorescence in both channels and therefore appear in yellow. Different patterns of activation can be observed at different frequencies, and GCaMP activity returns to baseline by 30 s post-stimulus. Scale = 100 µm. *k*=-0.12. b) GCaMP activity of labeled cells with increasing distances from the electrode (by distance from the electrode edge: 1 = 15 µm; 2 = 33 µm; 3 = 51 µm; 4 = 54 µm; 5 = 64 µm; and 6 = 105 µm). Horizontal lines indicate threshold. Neurons 1, 4, and 6 show electrical stimulation induced GCaMP activity above threshold while 2, 3, and 5 do not.

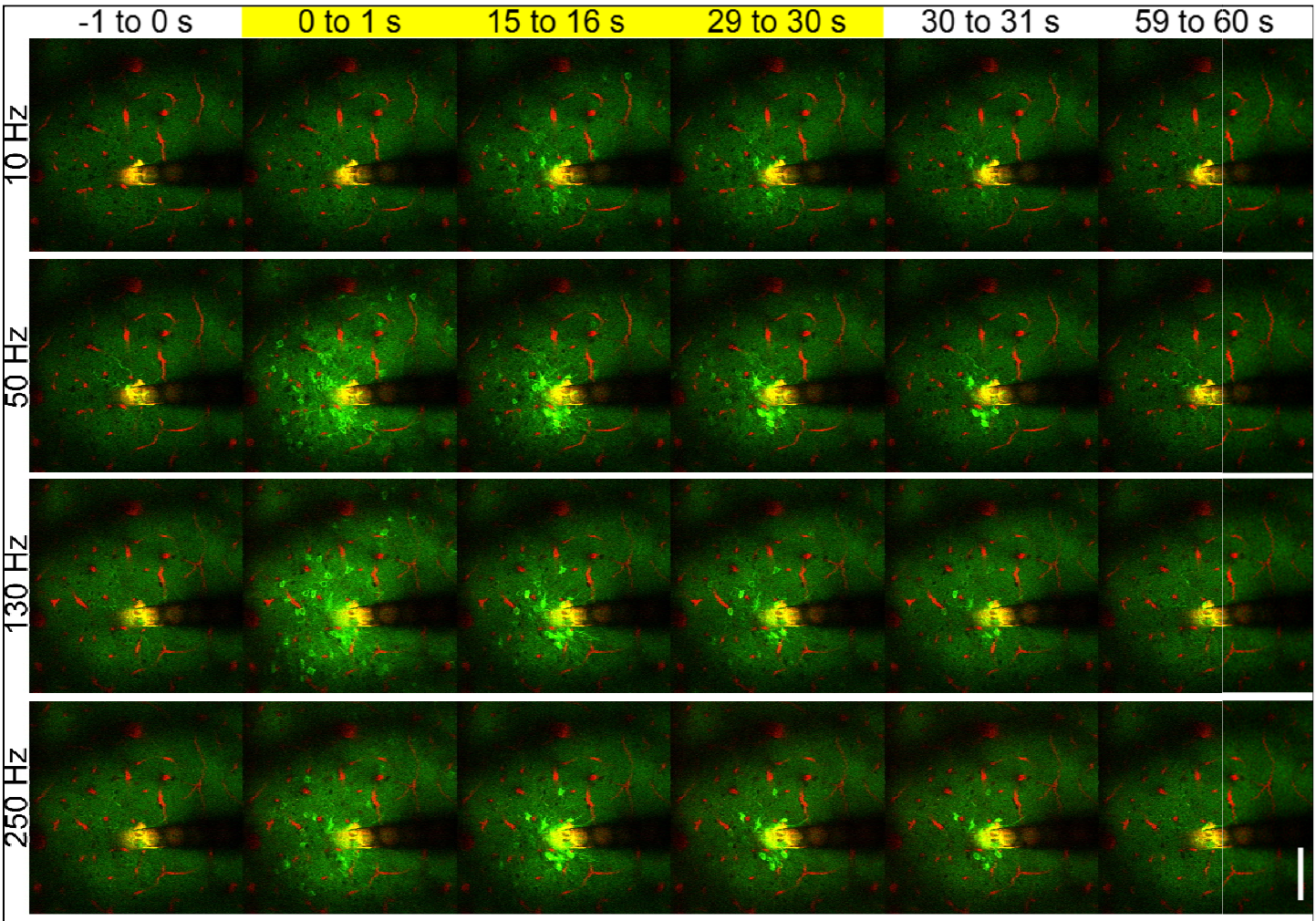

Figure 3: Continuous electrical stimulation evokes frequency dependent temporal activation. Mean GCaMP activity immediately before stimulation (-1 to 0s), at stimulation onset (0 to 1s), during stimulation (15 to 16s), immediately before stimulation termination (29 to 30s), immediately after termination (30 to 31s) and after stimulation (59 to 60 s). While the activation of GCaMP is lower at 10 Hz, GCaMP activation pattern is similar at onset across frequencies. However, the activation pattern at the end of the stimulation train (29 to 30 s) differs based on frequency of the stimulation. Images taken from the same animal and trials as figure 2. Scale = 100 µm. *k*=-0.12.

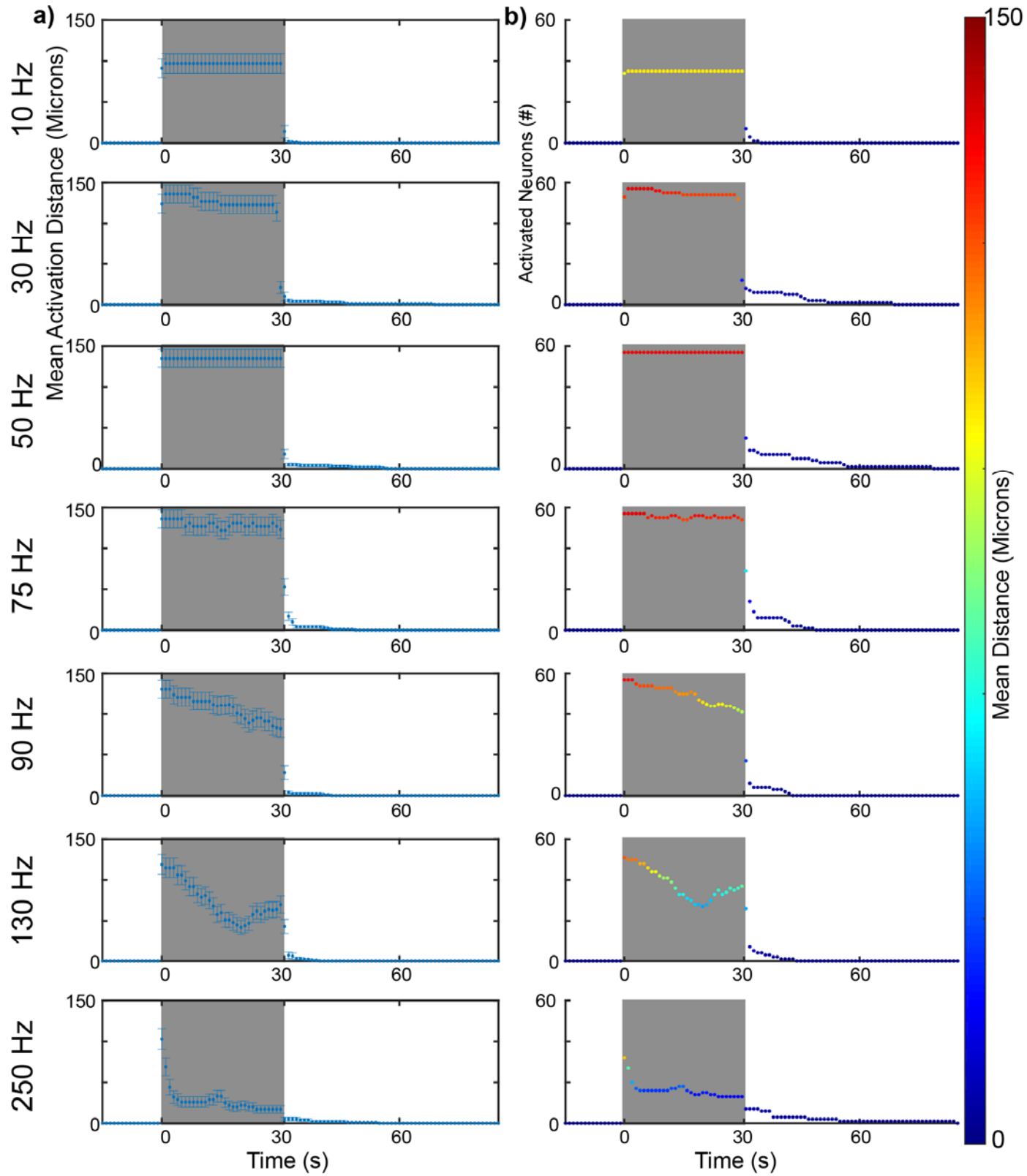

Figure 4: Spatial and temporal distribution of frequency dependent GCaMP activation in a representative animal. a) The average distance of all active neurons during electrical stimulation (grey box) decreases over time at higher frequencies. Error bars indicate standard error. **b)** The number of active neurons during electrical stimulation also decreases over time at higher frequencies. Mean activation distance from panel (a) is represented in color to show that electrical stimulation at higher frequencies (>90 Hz) leads to a decrease in the average distance of calcium activity over long stimulation pulse trains (color) and decrease in variance (a), suggesting the decrease in average distance is due to discontinued activity of distant neurons.

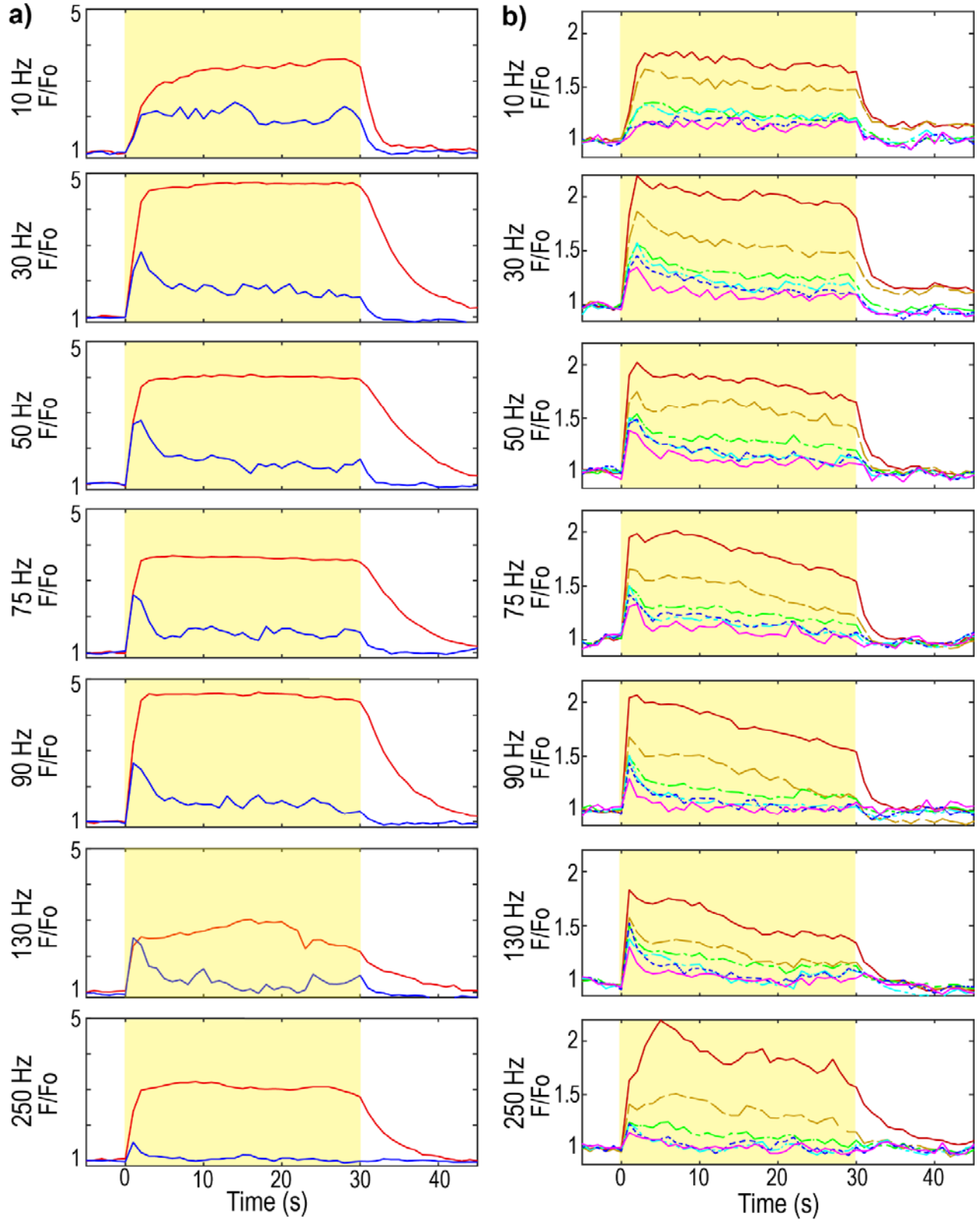

Figure 5: Neuronal soma activation and neuropil activation show frequency dependent temporal falloff. a) GCaMP activation in the soma at 15 µm (red) or 115 µm (blue) from the electrode site. Yellow indicates the stimulation. F_0 is the mean intensity of the pre-stimulus period. Calcium activity was averaged into 1 s bins to facilitate visualization. **b)** GCaMP neuropil activation at 10-20 µm (red, solid line), 30-40 µm (orange, dashed line), 50-60 µm (green, -·-), 100-110 µm (cyan, -···-), 150-160 µm (blue, dotted line), and 245-255 µm (violet, solid line) from the electrode site. Spatial and temporal neuropil falloff increase with frequency.

Distinct GCaMP intensity falloff between neuronal somas and neuropil during stimulation

Neuropil activation as a function of distance from the electrode, time post-stimulation onset, and frequency of stimulation was also examined (Fig. 5). Since the neuropil is composed of neurites from surrounding GCaMP-expressing cells, it is understood to represent a spatial average of nearby responding and non-responding cells (Histed et al., 2009). In this analysis, regions of interest previously identified as isolated somas were removed, and the average changes in GCaMP intensity in the remaining volume were assessed. Across all frequencies tested, there appears to be a near linear fall off in stimulation evoked GCaMP intensity as a function of distance from the electrode (Fig. 5b red vs orange vs green lines). In contrast to the neuropil, example neurons near (15 µm) the electrode site show gradual increase in GCaMP intensity at 10 Hz and a rapid plateau between 30 to 90 Hz (Fig. 5b, blue; 15 µm). However, similar to the time course of distant soma activation (Fig. 5b, red; 115 µm), there is a peak in activation of the neuropil in the first five seconds post stimulation, with a decrease in activation thereafter. At 10 Hz the decrease in neuropil activation is slower across all distances, with the peak and subsequent decay being steeper (slope of F/F_0) for higher frequencies. There is also a post-stimulus residual activation for both the neuropil and local neurons (Fig. 5a b). This residual increase in activation can last up to 30 seconds or more post stimulation (Fig. 4b) for somas, but is typically shorter in duration for the neuropil (Fig. 5a).

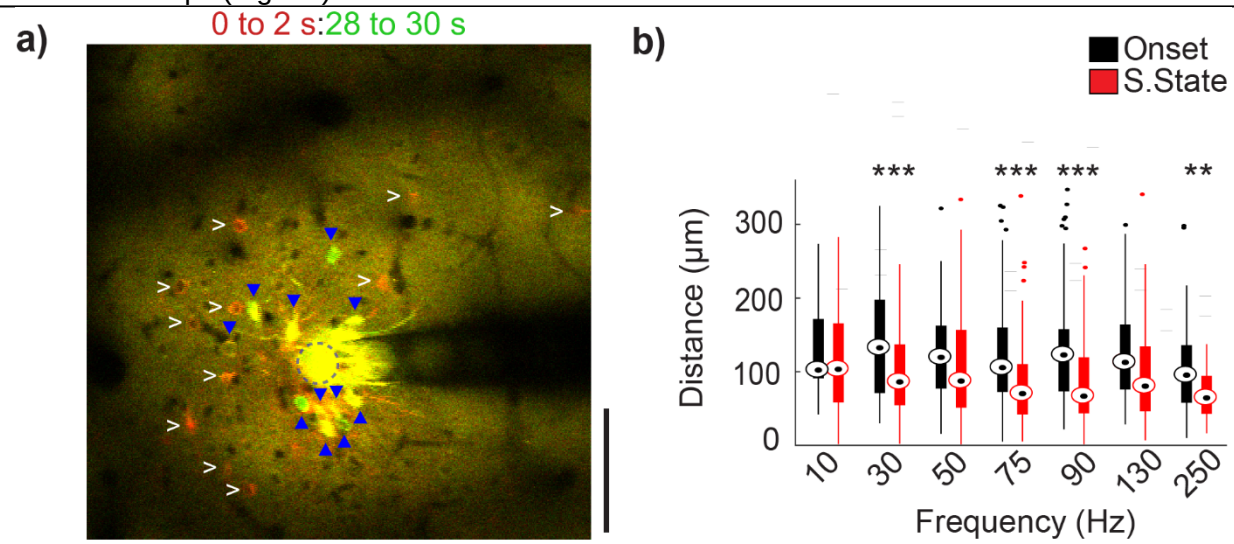

Figure 6: Onset and steady-state neurons are spatially distinct at high stimulation frequencies. (a) Mean GCaMP activity at the onset of the stimulation (0 to 2 s; red) and immediately before the end of stimulation (28 to 30 s; green) (stimulation parameter: 250 Hz, 50µA). Onset neurons (white arrowheads) and steady-state: (blue triangle) are marked in both images. Some steady-state neurons were also active at the onset of stimulation (yellow). (b) Average distance of the neurons activated during onset and steady-state phase. With increasing frequency, onset activated neurons are located significantly further from the electrode site than steady-state neurons. Repeated measures two-way ANOVA (within frequencies, n=15 neurons, $F=14.707$, $p<0.005$). Post-hoc t-tests with Bonferroni correction: **$p<0.01$ and ***$p<0.001$.

Stimulation in somatosensory cortex activates neurons with different temporal activation behavior

Previous work evaluating the effects of microstimulation on neuronal activation utilized brief stimulation paradigms with pulse train durations on the order of milliseconds (Histed et al., 2009). However, during continuous stimulation, different temporal activation patterns were observed during the stimulation period in individual mice (Figs 3 & 4). Therefore, the aggregate temporal properties of neuronal activation across all mice (n=5) was examined. Temporal activation was separated into 1) onset neurons that rapidly decline in activity during stimulation and 2) steady-state neurons that remain activated throughout the stimulation period. Somas were classified as onset-responsive if they were activated during the first 0-2 s of the 30 s pulse train but ceased activation before the final 2 s of the pulse train (28-30 s); or as steady-state-responsive neurons if they were active during the final 2 s of stimulation (28-30 s post-stimulation onset) (Fig. 6a). In these acute experiments, all steady-state neurons were also active in the first 2 s of the pulse train. The duration of onset and steady-state neuron activity was measured by quantifying the total time during the stimulation period that GCaMP intensity was greater than an intensity threshold of three standard deviations from the pre-stimulus period. Further, steady-state neurons had a significantly greater Activation Time than onset neurons

(Supplemental Fig. 2a, repeated measures two-way ANOVA with Bonferroni post-hoc comparison, F=374.831, p<0.001).

In order to evaluate if there was a spatial relationship for onset and steady-state somas, the spatial distribution of the two populations were compared (Fig. 6a). Since charge density accumulates on the edges of planar electrode sites, (Wei & Grill, 2009) distances were measured from the center of each soma to the nearest edge of the stimulating electrode site. Steady-state neurons were generally located closer to the electrode site than onset neurons, on average by ~40 µm (Fig. 6b). This phenomenon tended to occur at higher frequencies (Fig. 6b; at 130 Hz, p=0.058). Onset neurons and steady-state neurons showed distinct spatial relationships that were distal or proximal to the stimulation electrode, respectively.

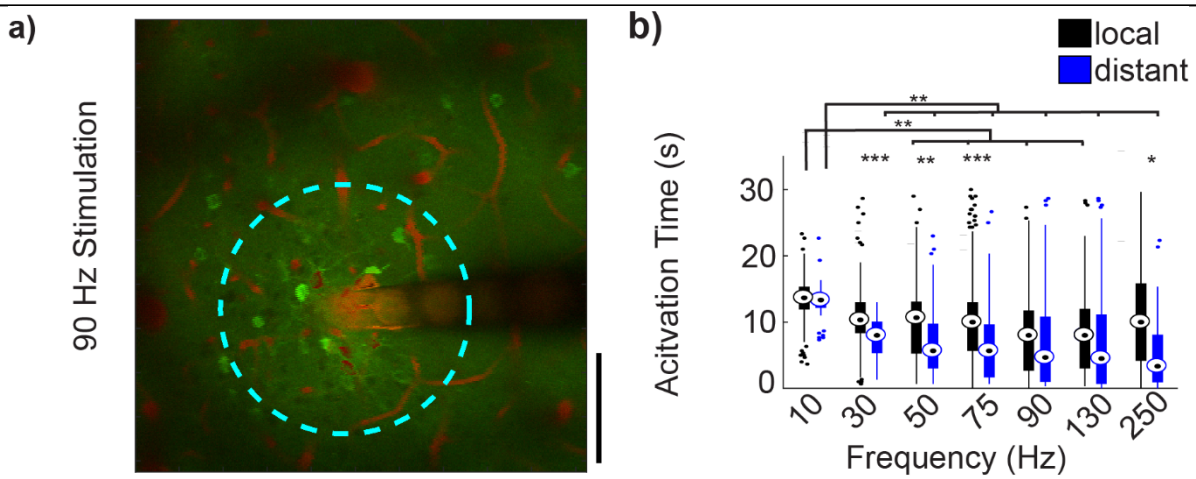

Figure 7: Activation properties of local and distant neuronal populations. (a) Standard deviation intensity projection over 30 seconds following 90Hz stimulation. Distance threshold shown by cyan circle. (b) Average activation time for local and distant activated neuron populations. Repeated measures two-way ANOVA (within frequencies, n=21 neurons, F=46.022, p<0.005; between frequencies F=10.483, p<0.005). Post-hoc t-tests with Bonferroni correction: *p<0.05 **p<0.01 and ***p<0.001.

Stimulation in somatosensory cortex activates local and distant neurons in a frequency dependent manner

During continuous electrical stimulation at higher frequencies, onset neurons that decreased in activity tended to be at a greater distance from the electrode compared to steady state neurons (Fig. 5). We also evaluated the opposite relationship; if GCaMP activity in distant somas decreased over long stimulus durations at higher frequencies. While stimulation frequencies greater than 50 Hz led to onset and steady-state neurons exhibiting a confined spatial spread (Fig. 6b), not all onset neurons were distant neurons, and not all distant neurons were steady-state neurons. Therefore, in order to minimize bias, somas were also grouped by distance to evaluate if 'local' and 'distant' neurons exhibited distinct temporal relationships. The aggregated temporal activation patterns over local and distant neuronal populations in all mice (n=5) were considered. Somas were spatially classified by establishing a distance threshold (see methods, Fig. 7a), whereby cell bodies located within the threshold were considered 'local' neurons, while cells located outside the threshold were considered 'distant' neurons. No significant differences were observed between the number of activated local or distant neurons (Supplemental Fig. 3a).

Somatic calcium changes generally reflect action potential firing; although during periods of high spike rates, GCaMP6 fluorescence intensity can saturate due to the long decay constant (Chen et al., 2013). Because somas may exhibit initially high stimulation-evoked firing rates, which can be followed by a period of lower activity throughout the rest of the stimulation period (Fig. 5b; red), measurements of the duration of activation did not effectively capture the dynamics of neuronal responses. Therefore, to evaluate if local and distant somas had different temporal activation patterns, the 'Activation Time' of the two populations were compared. The Activation Time was defined as an estimate of the mean time at which the cell is responsive, weighted by the GCaMP intensity, and was calculated as the time-point at which the cumulative intensity reached 50% of the sum of the total $\Delta F/F_0$ signal change during the stimulation period. Activation Time was significantly greater in local somas than in distant somas for 30 Hz (10.9±0.4 vs 7.6±0.4 s), 50 Hz (9.8±0.6 vs 6.9±0.7 s), 75 Hz

(10.5±0.6 vs 6.4±0.7 s), and 250 Hz (11.4±0.9 vs 5.7±1.5 s) stimulation (Fig. 7b, F=46.022, p<0.05). Additionally, Activation Time of both local and distant somas showed significant frequency dependence (Fig. 7b, F=10.482, p<0.001). Particularly of note was that for 10Hz stimulation, the local somas had significantly greater Activation Time than at higher stimulation frequencies (F=10.482, p<0.01).

As a spatial pattern of activation was observed during continuous stimulation (Fig 7b), the activation density for local and distant populations was measured. Activation density for local somas was calculated as the number of somas activated within the distance threshold, divided by the total area encompassed by the threshold. For distant somas, activation density was calculated using the area encompassed by an annulus with inner radius, *r*, equal to the distance threshold, and outer radius, *R*, equal to the distance of the furthest soma. For 10, 30, 75, and 90 Hz stimulation, local neurons had significantly greater neuronal density than distant somas (Supplemental Fig. 3b, F=2.993, p<0.05).

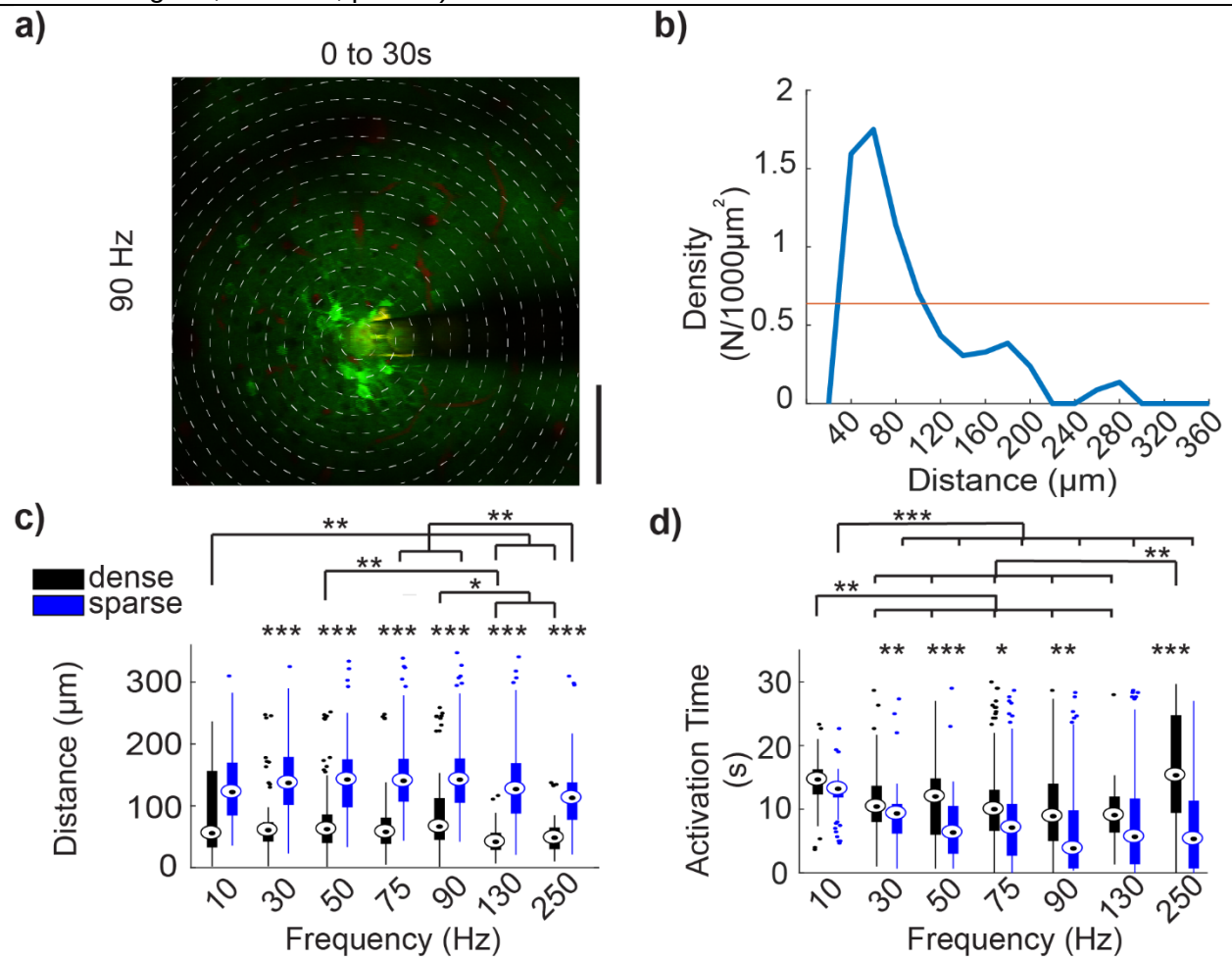

Figure 8: Activation properties of dense and sparse populations of neurons. (a) Mean GCaMP activity (30 s, 90 Hz stimulation) with concentric bins of 20 μm incremental radius around the center of the electrode site, demonstrating density calculation method. (b) For the same trial, density (N/1000 μm^2) is plotted against distance of the bins from the electrode. (c) Average distance of dense and sparse activated neurons. For all stimulation frequencies, sparsely activated neurons are located farther from the electrode site than dense activated neurons. (d) Average activation time of dense and sparse activated neuron population. Dense activated neurons are active for a longer duration in all stimulation frequency except 130Hz. Repeated measures two-way ANOVA (for (c) within frequencies: n=42 neurons, F=180.332, p<0.001; between frequencies: F=28.137, p<0.001. for (d) within frequencies: n=42 neurons, F=15.088, p<0.001; between frequencies: F=5.527, p<0.001). Post-hoc t-tests with Bonferroni correction: *p<0.05, **p<0.01 and ***p<0.001

Stimulation in somatosensory cortex creates a frequency dependent activation density pattern

In studies by Stoney et al, they noted activation of densely packed somas local to the electrode. In contrast, Histed et al noted only sparse activation of distant somas. To investigate this discrepancy, we evaluated the density of somas activated as a function of distance from the electrode. Prolonged electrical stimulation led to

a dense activation pattern characterized by a decrease in activity in distant somas at frequencies >10 Hz. As before, somas were then separated into dense and sparse populations using a density threshold and evaluated for distinct spatial and temporal relationships. In order to evaluate if continuous electrical stimulation can activate a set of cells restricted to a small spatial area, patterns of somatic activation were classified as dense or sparse. Concentric circular bins were drawn with their origin at the center of the electrode site with subsequent bins increasing in 20 µm radial increments (Fig. 8a). Density was calculated as the number of activated neurons in each bin, divided by the concentric bin area (Fig 8b). Density thresholds were established similarly to distance thresholds.

Activated somas within dense populations were located significantly closer to the electrode site for all stimulation frequencies except 10 Hz (Fig. 8c, $F=180.332$, $p<0.001$). Additionally, densely activated somas generally showed significantly greater Activation Times compared to sparsely activated somas (Fig. 8d, $F=15.088$, $p<0.05$). The Activation Time of dense and sparse somas showed similar frequency dependence as observed in local and distal somas in Fig. 7b. However, the Activation Time for dense neurons at 250 Hz stimulation was significantly greater than at stimulation frequencies tested from 30-130 Hz ($F=5.527$, $p<0.01$). Somas that were classified as higher density were closer to the electrode and had longer Activation Times compared to sparse cells, which were further from the electrode and had shorter Activation Times. At the onset of electrical stimulation, there was a low density, sparse, and distributed activation pattern of neurons.

Discussion:

This work shows that continuous electrical stimulation for 30 seconds in acute experiments strongly activated somas located in close proximity to the electrode for the duration of the stimulation period for frequencies >10 Hz (Figures 2-8). Previous work by Histed et al utilizing 2-photon microscopy and a calcium indicator demonstrated that stimulation with <1 s pulse trains of cathodic phase leading, 200 µs/phase, biphasic pulses under 10 µA in current at 250 Hz, resulted in a sparse, distributed population of activated neurons surrounding the electrode tip, without a strong bias towards neurons near the tip (Histed et al., 2009). Increasing current over the 4-9 µA range increased the density of neurons activated within this 100-200 µm sphere, again without a bias towards closer to the stimulation site (Histed et al., 2009). Through multiple experimental manipulations they concluded that stimulation in this confined parameter space only directly activates axons within 30 µm of the electrode, which in turn antidromically activates the somas associated with these axons, yielding the observed sparse pattern of somatic activation (Histed et al., 2009). These results were counter to prevailing theory based on seminal studies by Stoney et al which suggest that stimulation leads to a sphere of activated neurons near the electrode tip, with the size of the sphere growing in proportion to the current applied (Murasugi, Salzman, & Newsome, 1993; Ranck, 1975; Rattay, 1999; Robinson & Fuchs, 1969; Stoney Jr et al., 1968; Tehovnik, 1996; Tolias et al., 2005).

The Histed results were obtained using stimulation charges at or just above the threshold for eliciting a significant response using a calcium indicator (0.8 to 1.8 nC/phase), applied for brief periods (<1 s) and at very high frequency (250 Hz), which led to the implication that, “it is impossible to activate a set of cells restricted to a small spatial volume” (Histed et al., 2009). In contrast, the results described in our study using longer pulse trains (30 s) and larger stimulation charges (2.5 nC/phase) show a distinct pattern of somatic activation across frequencies consisting of a comparatively denser group of somas near the electrode tip and a sparse group of neurons located distant from the electrode. In short, our results support both the original studies by Stoney and the more recent study by Histed, painting a complex picture of spatial activation that is dependent on charge applied and time of observation during an extended pulse train (Histed et al., 2009; Stoney Jr et al., 1968).

The data in the present study demonstrate that, in general, activated somas both local and distant remain activated at lower stimulation frequencies throughout the duration of the pulse train. At higher frequencies (90 Hz and above), distant somas activated at the beginning of the 30 s pulse train cease to remain active by the end of the pulse train, with the Activation Time progressively shorter as the frequency was increased. The responses of local axons versus somas also differentially changed over the course of an extended pulse train, where frequencies over 50 Hz lead to initial transient activation that eventually subsides over the course of the pulse train.

The idea that different elements of the neuron may be activated or inactivated at different applied currents is not new (Cameron C McIntyre & Grill, 2002; Overstreet, Klein, & Tillery, 2013). It is often assumed, however, that at frequencies at which pulse to pulse entrainment is feasible (130 Hz or less), the differential evoked responses local to the electrode are primarily a function of charge applied (current*pulsewidth), given that stimulation is within the Shannon/McCreery safety limits (Cogan et al., 2016; Shannon, 1992). In this paradigm, changes in evoked network response as a function of frequency and time over the duration of pulse train have been presumed to be presynaptically mediated, e.g. vesicular depletion at the synapse leading to synaptic depression (Y. Wang & Manis, 2008). However, stimulation of CA1 neurons via antidromic activation of efferent fibers exhibits time-varying responses, where the transient population response at the onset of stimulation exceeds steady state activity during stimulation (Cai et al., 2017). Notably, the magnitude of the antidromically evoked population responses was found to be frequency dependent, where higher frequencies of stimulation elicited weaker onset and steady state responses. Moreover, high frequency stimulation of axons at 100 and 200 Hz disrupts the synchronicity of evoked neuronal responses compared to 50 Hz (Z. Wang, Feng, & Wei, 2018). Very high frequency stimulation (~10 kHz) can block neural activity altogether in isolated fibers in the periphery. While McCreery et al. has demonstrated that continuous stimulation for periods of only seven hours can lead to Stimulation Induced Depression of Neuronal Excitability (SIDNE) (D. B. McCreery, Agnew, & Bullara, 2002; D. B. McCreery, Yuen, Agnew, & Bullara, 1997), and other studies have shown that continuous stimulation for as short as 1 hr/day could lead to significantly different behavioral outcomes (Hao et al., 2015; White & Sillitoe, 2017), the activation and then subsequent decrease of activation in local axons and their connected soma over the course of a much shorter 30 second pulse train, suggests an underlying mechanism that has not been previously explored.

The mechanism by which increasing frequency may cause transient activation of axons local to the electrode followed by inactivation over the pulse train is presently not understood. Continuous stimulation could cause intermittent failure to propagate action potentials through the axon at frequencies as low as 30 Hz, putatively mediated by extracellular accumulation of K^+ ions, depletion of ATP, and reduced inward Na^+ current (Smith, 1980). Alternatively, it is possible that increasing frequency could lead to virtual anode generation. Increasing intensities of cathodic stimulation may generate a virtual anode which hyperpolarizes membranes on stimulated fibers distant from the cathode, and blocks the propagation of action potentials initiated near the cathode (Ranck, 1975). Due to the capacitive nature of the electrode-electrolyte interface and the lipid bilayer of the neural element (Bates & Chu, 1992), increasing stimulation frequency at a fixed amplitude will yield a lower impedance that may facilitate virtual anode generation. Further studies are necessary to better understand the cause of inhibition of calcium activity in distal somas at higher frequencies.

Under normal conditions, neuronal depolarization causes an influx of intracellular calcium through pathways such as voltage or neurotransmitter gated Ca^{2+} channels, which is measured by the GCaMP indicator (Berridge, 1998). The calcium influx then leads to Ca^{2+} release through channels present in intracellular stores, mainly the endoplasmic reticulum (Sharp et al., 1993). Intracellular calcium can then induce local changes at the synaptic level or regulate gene expression (Berridge, 1998). However, excessive levels of intracellular calcium can have neurotoxic effects (Arundine & Tymianski, 2003). We observed activated cells near the stimulating electrode site with sustained GCaMP fluorescence without having discernable spikes (as observed in the plateau in fluorescence change in Fig. 5). This may be due to the simultaneous activation of inhibitory neurons (non-GCaMP expressing) (Dana et al., 2014). Nevertheless, the long-term impact that sustained intracellular calcium concentrations induced by microstimulation may have on local gene expression, synaptic properties, and neuronal health remains to be elucidated. For example, continuous stimulation at parameters above the safety limits (k>1.7~1.85) established by the Shannon curve can cause damage to tissue in the vicinity of the electrode, which is often attributed to driving toxic electrochemical reactions at the surface of the electrode, or driving local neural tissue to increase activity beyond physiological norms leading to excitotoxic effects (Agnew, Yuen, Pudenz, & Bullara, 1975; Cogan et al., 2016; Merrill, Bikson, & Jefferys, 2005; Mortimer, Shealy, & Wheeler, 1970; Shannon, 1992; Yuen, Agnew, Bullara, Jacques, & McCreery, 1981). Furthermore, pioneering work by McCreery suggests that 4 nC/phase represents a stimulation threshold above which obvious damage occurs, as assessed by gross histological metrics, as opposed to larger electrodes which are governed by the Shannon equation (D. McCreery, Pikov, & Troyk, 2010; Douglas B McCreery, Agnew, Yuen, & Bullara, 1990). While this present study was carried out below the Shannon limit and charge density per phase outlined by McCreery, the biological substrates of plasticity induced by clinically relevant stimulation parameters over time remain poorly understood.

Additionally, various studies have demonstrated that electrical stimulation can cause diverse effects such as increases in hippocampal and thalamic volume, increases in blood vessel size and synaptic density, cortical dendrite growth, and changes in mRNA expression - some of which may influence short term local somatic and axonal response (Agnew et al., 1975; Baudry, Oliver, Creager, Wieraszko, & Lynch, 1980; Brownson, Little, Jarvis, & Salmons, 1992; Chakravarty et al., 2016; Cooperrider et al., 2014; Gall, Murray, & Isackson, 1991; Hirano, Becker, & Zimmerman, 1970; Morris, Feasey, ten Bruggencate, Herz, & Hollt, 1988; Pudenz, Bullara, Dru, & Talalla, 1975; Sankar et al., 2015; Sankar et al., 2016; Veerakumar et al., 2014; Xia, Buja, Scarpulla, & McMillin, 1997; Xia et al., 2000). In chronic neuromodulation or neuroprosthetic applications, additional complexities arise from tissue changes in both the neuronal and non-neuronal populations due to the implantation injury (glia, neurovasculature, immune cells) (Kolarcik et al., 2015; Takashi Daniel Yoshida Kozai, Jaquins-Gerstl, Vazquez, Michael, & Cui, 2015; Michelson et al., 2018; Salatino, Ludwig, Kozai, & Purcell, 2017; Steven M. Wellman & Kozai, 2017), electrode material degradation (Alba, Du, Catt, Kozai, & Cui, 2015; Cogan, 2008; Cogan et al., 2016; T. Kozai et al., 2014; Steven M Wellman et al., 2018; Wilks et al., 2017), and plastic changes from long-term electrical stimulation (Agnew et al., 1975; Baudry et al., 1980; Brownson et al., 1992; Chakravarty et al., 2016; Cooperrider et al., 2014; Gall et al., 1991; Hirano et al., 1970; Merrill et al., 2005; Morris et al., 1988; Pudenz et al., 1975; Sankar et al., 2015; Sankar et al., 2016; Veerakumar et al., 2014; Xia et al., 1997; Xia et al., 2000). Future studies should be aimed at disentangling the complex network of dendrites, axons, and cell bodies of inhibitory and excitatory cells that may be present near the electrode in the brain (Overstreet et al., 2013).

The frequency dependent inactivation of axons local to the electrode over the course of an extended pulse train may provide insight on a potential mechanism of action for electrical stimulation for specific therapeutic uses (Agnesi, Muralidharan, Baker, Vitek, & Johnson, 2015; Gildenberg, 2005). For example, as DBS of the subthalamic nucleus (STN) to treat the tremor associated with Parkinson's Disease was originally based on the positive results of lesioning the same area, STN DBS was originally thought to generate the equivalent of a titratable/reversible lesion of STN. Following studies utilizing microwires for electrophysiological recordings - which are biased towards sampling action potentials initiated at the axon hillock, as this is where the largest current deflection occurs – suggested that therapeutic DBS parameters in the 130 Hz range differentially suppress the activity of local STN somas while still activating local axons projecting to the targets from STN nuclei (Cameron C. McIntyre, Grill, Sherman, & Thakor, 2004). This led to the suggestion that DBS may be creating an information lesion of signals passing through STN, as entrainment at 130 Hz would prevent the passage of physiological signals with any temporal information, due to the stimulus rate and the absolute and relative refractory period of a neuron (Agnesi, Connolly, Baker, Vitek, & Johnson, 2013; Grill, Snyder, & Miocinovic, 2004). More recently antidromic activation of tracks of passage traveling near STN from motor cortex, known as the hyperdirect pathway, have received increasing attention as a potential mechanism to ameliorate pathological thalamocortical oscillations driving tremor in Parkinson's Disease (Gradinaru, Mogri, Thompson, Henderson, & Deisseroth, 2009; Li, Arbuthnott, Jutras, Goldberg, & Jaeger, 2007; Cameron C McIntyre & Hahn, 2010). In contrast, 10 Hz optogenetic stimulation in the brain leads to the highest probability of entrainment, with the entrainment probability significantly decreasing at frequencies greater than 15 Hz (Bitzenhofer et al., 2017). Therefore, it may not be surprising that 10 Hz electrical stimulation leads to continuous GCaMP activity over long stimulus pulse trains. The results in the present study demonstrate that stimulation at high frequencies associated with therapeutic DBS initially activates both local soma and local axons connected to distant somas, but over time the evoked activity in local axons projecting to distant somas decreases. These data suggest that to understand the post-synaptic response to stimulation - and ultimately the therapeutic mechanisms of action - one must account for differential activation of axons vs somas near the electrode, as well as changes in the local activation profile as a function of frequency and time.

Limitations: Although care was taken to allow neuronal fluorescence intensities to return to pre-stimulation levels before another frequency was tested, stimulation frequencies were evaluated in increasing frequencies instead of randomizing the frequency order. Future studies should randomize one stimulation frequency to each implant location as well as evaluate the impact of the total number of stimulation pulses compared to stimulation frequency on driving stimulation induced depression of neuronal excitability. However, in two animals, 10 Hz trials were repeated after the entire frequency sequence and remained consistent with the first 10 Hz trial. Another key limitation is that calcium activity was observed under ketamine anesthesia, which inhibits NMDA receptors and potentiates $GABA_A$ receptors (Alkire, Hudetz, & Tononi, 2008), and shifts the

balance of excitatory and inhibitory transmission in cortex (Haider, Hausser, & Carandini, 2013; Homayoun & Moghaddam, 2007; Michelson & Kozai, 2018). These changes in neuronal excitability and network activity might potentially impact the frequency dependent responses to microstimulation observed here. Finally, all experiments were carried out on male mice in this limited scope study. Future work will include comparisons to female mice.

Conclusion

Despite the widespread use of electrical stimulation as a scientific tool and a modality to affect therapeutic outcomes, a lack in understanding of its effects on network-level neural activity has limited its applicability. Without complete understanding of how an exogenous electric field is interacting with neuronal and non-neuronal cells local to a chronically implanted electrode at the targeted point of intervention - and activating or inhibiting individual elements of these cells types – it is difficult to understand the mechanism by which targeted electrical stimulation may be creating desired therapeutic outcomes or undesirable side effects. While the present work is not a complete study on the large parameter space of electrical stimulation, we disprove the hypothesis that the sparse and distributed neural activation patterns occur under continuous stimulation in a frequency independent manner. Instead, different stimulation parameters can dramatically alter the activation pattern at the cellular level in cortex. A deeper understanding of electrical stimulation parameters on neuronal activation (and non-neuronal activation) will be critical in utilizing electrical stimulation for targeted applications in basic science research as well as clinical therapeutics. Thus, the current work motivates additional non-clinical, non-translational basic science research to elucidate the mechanisms governing electrical stimulation.

Acknowledgements:
We thank Riazul Islam for assistance with neuron ROI selection, and James Trevathan and Evan Nicolai from the Mayo Clinic for helpful discussions. This work was supported by NIH NINDS R01NS094396, R01NS094404, R01NS062019, R01NS089688, and R21NS108098.

Conflict of Interest Statement:
The authors declare no competing interests.

Author Contributions:
All authors had full access to all the data in the study and take responsibility for the integrity of the data and the accuracy of the data analysis. *Conceptualization*, T.D.Y.K., A.L.V., and K.A.L.; *Methodology*, N.J.M. and T.D.Y.K.; *Investigation,* J.R.E. and T.D.Y.K.; *Formal Analysis*, N.J.M. and J.R.E.; *Writing – Original Draft*, T.D.Y.K., K.A.L., and N.J.M.; *Writing – Review & Editing*, all authors; *Visualization*, N.J.M., and T.D.Y.K.; *Supervision*, T.D.Y.K.; *Funding Acquisition*, T.D.Y.K.

References

Adrian, E. D. (1928). *The basis of sensation*: Christophers; London, 22 Berners Steeet, W. 1.

Adrian, E. D., & Bronk, D. W. (1928). The discharge of impulses in motor nerve fibres: Part I. Impulses in single fibres of the phrenic nerve. *The Journal of Physiology, 66*(1), 81.

Adrian, E. D., & Matthews, R. (1928). The action of light on the eye. *The Journal of Physiology, 65*(3), 273-298.

Agnesi, F., Connolly, A. T., Baker, K. B., Vitek, J. L., & Johnson, M. D. (2013). Deep brain stimulation imposes complex informational lesions. *PLoS One, 8*(8), e74462.

Agnesi, F., Muralidharan, A., Baker, K. B., Vitek, J. L., & Johnson, M. D. (2015). Fidelity of frequency and phase entrainment of circuit-level spike activity during DBS. *Journal of neurophysiology, 114*(2), 825-834.

Agnew, W. F., Yuen, T. G., Pudenz, R. H., & Bullara, L. A. (1975). Electrical stimulation of the brain. IV. Ultrastructural studies. *Surgical neurology, 4*(5), 438-448.

Alba, N. A., Du, Z. J., Catt, K. A., Kozai, T. D. Y., & Cui, X. T. (2015). In vivo electrochemical analysis of a PEDOT/MWCNT neural electrode coating. *Biosensors, 5*, 618-646. doi:10.3390/bios5040618

Alberts, W. W., Feinstein, B., Levin, G., Wright Jr, E., Darland, M., & Scott, E. (1965). Stereotaxic surgery for Parkinsonism: clinical results and stimulation thresholds. *Journal of Neurosurgery, 23*(2), 174-183.

Alkire, M. T., Hudetz, A. G., & Tononi, G. (2008). Consciousness and anesthesia. *Science, 322*(5903), 876-880. doi:10.1126/science.1149213

Arundine, M., & Tymianski, M. (2003). Molecular mechanisms of calcium-dependent neurodegeneration in excitotoxicity. *Cell Calcium, 34*(4-5), 325-337.

Bates, J. B., & Chu, Y. T. (1992). Electrode-electrolyte interface impedance: Experiments and model. *Annals of Biomedical Engineering, 20*(3), 349-362. doi:10.1007/bf02368536

Baudry, M., Oliver, M., Creager, R., Wieraszko, A., & Lynch, G. (1980). Increase in glutamate receptors following repetitive electrical stimulation in hippocampal slices. *Life sciences, 27*(4), 325-330.

Berridge, M. J. (1998). Neuronal calcium signaling. *Neuron, 21*(1), 13-26.

Bitzenhofer, S. H., Ahlbeck, J., Wolff, A., Wiegert, J. S., Gee, C. E., Oertner, T. G., & Hanganu-Opatz, I. L. (2017). Layer-specific optogenetic activation of pyramidal neurons causes beta-gamma entrainment of neonatal networks. *Nat Commun, 8*, 14563. doi:10.1038/ncomms14563

Brownson, C., Little, P., Jarvis, J. C., & Salmons, S. (1992). Reciprocal changes in myosin isoform mRNAs of rabbit skeletal muscle in response to the initiation and cessation of chronic electrical stimulation. *Muscle & nerve, 15*(6), 694-700. doi:10.1002/mus.880150611

Cai, Z., Feng, Z., Guo, Z., Zhou, W., Wang, Z., & Wei, X. (2017). Novel Stimulation Paradigms with Temporally-Varying Parameters to Reduce Synchronous Activity at the Onset of High Frequency Stimulation in Rat Hippocampus. *Front Neurosci, 11*, 563. doi:10.3389/fnins.2017.00563

Chakravarty, M. M., Hamani, C., Martinez-Canabal, A., Ellegood, J., Laliberte, C., Nobrega, J. N., . . . Lerch, J. P. (2016). Deep brain stimulation of the ventromedial prefrontal cortex causes reorganization of neuronal processes and vasculature. *Neuroimage, 125*, 422-427. doi:10.1016/j.neuroimage.2015.10.049

Chen, T. W., Wardill, T. J., Sun, Y., Pulver, S. R., Renninger, S. L., Baohan, A., . . . Kim, D. S. (2013). Ultrasensitive fluorescent proteins for imaging neuronal activity. *Nature, 499*(7458), 295-300. doi:10.1038/nature12354

Cogan, S. F. (2008). Neural Stimulation and Recording Electrodes. *Annual Review of Biomedical Engineering, 10*(1), 275-309. doi:doi:10.1146/annurev.bioeng.10.061807.160518

Cogan, S. F., Ludwig, K. A., Welle, C. G., & Takmakov, P. (2016). Tissue damage thresholds during therapeutic electrical stimulation. *Journal of Neural Engineering, 13*(2), 021001.

Cooperrider, J., Furmaga, H., Plow, E., Park, H. J., Chen, Z., Kidd, G., . . . Machado, A. G. (2014). Chronic deep cerebellar stimulation promotes long-term potentiation, microstructural plasticity, and reorganization of perilesional cortical representation in a rodent model. *The Journal of neuroscience : the official journal of the Society for Neuroscience, 34*(27), 9040-9050. doi:10.1523/JNEUROSCI.0953-14.2014

Cushing, H. (1909). A note upon the faradic stimulation of the postcentral gyrus in conscious patients. *Brain, 32*(1), 44-53.

Dana, H., Chen, T. W., Hu, A., Shields, B. C., Guo, C., Looger, L. L., . . . Svoboda, K. (2014). Thy1-GCaMP6 transgenic mice for neuronal population imaging in vivo. *PLoS One, 9*(9), e108697. doi:10.1371/journal.pone.0108697

De Balthasar, C., Boex, C., Cosendai, G., Valentini, G., Sigrist, A., & Pelizzone, M. (2003). Channel interactions with high-rate biphasic electrical stimulation in cochlear implant subjects. *Hear Res, 182*(1-2), 77-87.

Delgado, J. M., Hamlin, H., & Chapman, W. P. (1952). Technique of intracranial electrode implacement for recording and stimulation and its possible therapeutic value in psychotic patients. *Confin Neurol, 12*(5-6), 315-319.

Djourno, A., Eyries, C., & Vallancien, B. (1957). DE LEXCITATION ELECTRIQUE DU NERF COCHLEAIRE CHEZ LHOMME, PAR INDUCTION A DISTANCE A LAIDE DUN MICRO-BOBINAGE INCLUS A DEMEURE. *Comptes Rendus des Séances de la Société de Biologie et de ses Filiales, 151*(3), 423-425.

Dobelle, W., & Mladejovsky, M. (1974). Phosphenes produced by electrical stimulation of human occipital cortex, and their application to the development of a prosthesis for the blind. *The Journal of physiology, 243*(2), 553-576.

Dobelle, W. H., Mladejovsky, M. G., & Girvin, J. P. (1974). Artifical vision for the blind: electrical stimulation of visual cortex offers hope for a functional prosthesis. *Science, 183*(4123), 440-444.

Doyle Jr, J., Doyle, J., Turnbull, F., Abbey, J., & House, L. (1963). ELECTRICAL STIMULATION IN EIGHTH NERVE DEAFNESS. A PRELIMINARY REPORT. *Bulletin of the Los Angeles Neurological Society, 28*, 148.

Du Bois-Reymond, E. H. (1884). *Untersuchungen über thierische elektricität: bd., 1. abth* (Vol. 2): G. Reimer.

Eccles, J. C. (1953). The neurophysiological basis of mind: the principles of neurophysiology.

Eles, J. R., Kozai, T. D. Y., Vazquez, A. L., & Cui, X. T. (2018). In vivo imaging of neuronal calcium during electrode implantation: spatial and temporal mapping of damage and recovery. *Biomaterials*.

Eles, J. R., Vazquez, A. L., Snyder, N. R., Lagenaur, C. F., Murphy, M. C., Kozai, T. D. Y., & Cui, X. T. (2017). Neuroadhesive L1 coating attenuates acute microglial attachment to neural electrodes as revealed by live two-photon microscopy. *Biomaterials, 113*, 279-292.

Flesher, S. N., Collinger, J. L., Foldes, S. T., Weiss, J. M., Downey, J. E., Tyler-Kabara, E. C., . . . Gaunt, R. A. (2016). Intracortical microstimulation of human somatosensory cortex. *Science translational medicine, 8*(361), 361ra141-361ra141.

Fritsch, G., & Hitzig, E. (1870). Ueber die elektrische Erregbarkeit des Grosshirns. Archiv fur Anatomie und Physiologie und wissenschaftliche Medizin. *37*, 300–332. .

Gall, C., Murray, K., & Isackson, P. J. (1991). Kainic acid-induced seizures stimulate increased expression of nerve growth factor mRNA in rat hippocampus. *Brain research. Molecular brain research, 9*(1-2), 113-123.

Galvani, L. (1791). D viribus electricitatis in motu musculari: Commentarius. *Bologna: Tip. Istituto delle Scienze, 1791; 58 p.: 4 tavv. ft; in 4.; DCC. f. 70*.

Galvani, L., & Aldini, G. (1792). *Aloysii Galvani... De viribus electricitatis in motu musculari commentarius cum Ioannis Aldini Dissertatione et notis. Accesserunt Epistolæ ad animalis electricitatis theoriam pertinentes*: Apud Societatem Typographicam.

Gildenberg, P. L. (2005). Evolution of neuromodulation. *Stereotactic and functional neurosurgery, 83*(2-3), 71-79.

Gol, A. (1967). Relief of pain by electrical stimulation of the septal area. *Journal of the neurological sciences, 5*(1), 115-120.

Gradinaru, V., Mogri, M., Thompson, K. R., Henderson, J. M., & Deisseroth, K. (2009). Optical deconstruction of parkinsonian neural circuitry. *Science, 324*(5925), 354-359.

Greenberg, D. S., Houweling, A. R., & Kerr, J. N. D. (2008). Population imaging of ongoing neuronal activity in the visual cortex of awake rats. *Nat Neurosci, 11*, 749-751. doi:10.1038/nn.2140

Grill, W. M., Snyder, A. N., & Miocinovic, S. (2004). Deep brain stimulation creates an informational lesion of the stimulated nucleus. *Neuroreport, 15*(7), 1137-1140.

Haider, B., Hausser, M., & Carandini, M. (2013). Inhibition dominates sensory responses in the awake cortex. *Nature, 493*(7430), 97-100. doi:10.1038/nature11665

Hao, S., Tang, B., Wu, Z., Ure, K., Sun, Y., Tao, H., . . . Samaco, R. C. (2015). Forniceal deep brain stimulation rescues hippocampal memory in Rett syndrome mice. *Nature, 526*(7573), 430.

Hassler, R., Riechert, T., Mundinger, F., Umbach, W., & Ganglberger, J. (1960). Physiological observations in stereotaxic operations in extrapyramidal motor disturbances. *Brain, 83*(2), 337-350.

Hirano, A., Becker, N. H., & Zimmerman, H. M. (1970). The use of peroxidase as a tracer in studies of alterations in the blood-brain barrier. *Journal of the neurological sciences, 10*(3), 205-213.

Histed, M. H., Bonin, V., & Reid, R. C. (2009). Direct activation of sparse, distributed populations of cortical neurons by electrical microstimulation. *Neuron, 63*(4), 508-522. doi:10.1016/j.neuron.2009.07.016

Hodgkin, A. L., & Huxley, A. F. (1952). A quantitative description of membrane current and its application to conduction and excitation in nerve. *J Physiol, 117*(4), 500-544.

Homayoun, H., & Moghaddam, B. (2007). NMDA receptor hypofunction produces opposite effects on prefrontal cortex interneurons and pyramidal neurons. *J Neurosci, 27*(43), 11496-11500. doi:10.1523/JNEUROSCI.2213-07.2007

House, L. R. (1987). Cochlear implant: the beginning. *Laryngoscope, 97*(8 Pt 1), 996-997.

House, W. F. (1976). Cochlear implants. *Ann Otol Rhinol Laryngol, 85 suppl 27*(3Pt2), 1-93.

Kent, A., & Grill, W. (2012). Recording evoked potentials during deep brain stimulation: development and validation of instrumentation to suppress the stimulus artefact. *Journal of Neural Engineering, 9*(3), 036004.

Kerr, J. N., & Denk, W. (2008). Imaging in vivo: watching the brain in action. *Nature Reviews Neuroscience, 9*(3), 195.

Kim, S., Callier, T., Tabot, G. A., Gaunt, R. A., Tenore, F. V., & Bensmaia, S. J. (2015). Behavioral assessment of sensitivity to intracortical microstimulation of primate somatosensory cortex. *Proceedings of the National Academy of Sciences, 112*(49), 15202-15207.

Kolarcik, C. L., Catt, K., Rost, E., Albrecht, I. N., Bourbeau, D., Du, Z., . . . Cui, X. T. (2015). Evaluation of poly(3,4-ethylenedioxythiophene)/carbon nanotube neural electrode coatings for stimulation in the dorsal root ganglion. *Journal of Neural Engineering, 12*, 016008. doi:10.1088/1741-2560/12/1/016008

Kozai, T., Alba, N., Zhang, H., Kotov, N., Gaunt, R., & Cui, X. (2014). Nanostructured Coatings for Improved Charge Delivery to Neurons. In M. D. Vittorio, L. Martiradonna, & J. Assad (Eds.), *Nanotechnology and Neuroscience: Nano-electronic, Photonic and Mechanical Neuronal Interfacing* (pp. 71-134). New York, NY: Springer New York.

Kozai, T. D., Vazquez, A. L., Weaver, C. L., Kim, S. G., & Cui, X. T. (2012). In vivo two-photon microscopy reveals immediate microglial reaction to implantation of microelectrode through extension of processes. *J Neural Eng, 9*(6), 066001. doi:10.1088/1741-2560/9/6/066001

Kozai, T. D. Y., Eles, J. R., Vazquez, A. L., & Cui, X. T. (2016). Two-photon imaging of chronically implanted neural electrodes: Sealing methods and new insights. *Journal of neuroscience methods, 256*, 46-55. doi:http://dx.doi.org/10.1016/j.jneumeth.2015.10.007

Kozai, T. D. Y., Jaquins-Gerstl, A., Vazquez, A. L., Michael, A. C., & Cui, X. T. (2015). Brain Tissue Responses to Neural Implants Impact Signal Sensitivity and Intervention Strategies. *ACS Chemical Neuroscience, 6*(1), 48-67. doi:10.1021/cn500256e

Kozai, T. D. Y., Jaquins-gerstl, A. S., Vazquez, A. L., Michael, A. C., & Cui, X. T. (2016). Dexamethasone retrodialysis attenuates microglial response to implanted probes in vivo. *Biomaterials, 87*, 157-169. doi:10.1016/j.biomaterials.2016.02.013

Kozai, T. D. Y., Marzullo, T. C., Hooi, F., Langhals, N. B., Majewska, A. K., Brown, E. B., & Kipke, D. R. (2010). Reduction of neurovascular damage resulting from microelectrode insertion into the cerebral cortex using in vivo two-photon mapping. *J Neural Eng, 7*(4), 046011. doi:S1741-2560(10)46092-9 [pii] 10.1088/1741-2560/7/4/046011

Li, S., Arbuthnott, G. W., Jutras, M. J., Goldberg, J. A., & Jaeger, D. (2007). Resonant antidromic cortical circuit activation as a consequence of high-frequency subthalamic deep-brain stimulation. *Journal of Neurophysiology, 98*(6), 3525-3537.

LifeScienceAlley. (2015). *LifeScience Alley Neuromodulation Sector Report* Retrieved from https://issuu.com/lifesciencealley/docs/neuromod-issuu:

Lilly, J. C., Hughes, J. R., Alvord, E. C., Jr., & Galkin, T. W. (1955). Brief, noninjurious electric waveform for stimulation of the brain. *Science, 121*(3144), 468-469.

Marcos, V., Francisco, V., Luisa, V. A., Bernardo, B., Fiacro, J., Francisco, B., & Irma, M. (2000). Subacute Electrical Stimulation of the Hippocampus Blocks Intractable Temporal Lobe Seizures and Paroxysmal EEG Activities. *Epilepsia, 41*(2), 158-169. doi:doi:10.1111/j.1528-1157.2000.tb00135.x

Mayer, D. J., & Liebeskind, J. C. (1974). Pain reduction by focal electrical stimulation of the brain: an anatomical and behavioral analysis. *Brain Research, 68*(1), 73-93.

McCreery, D., Pikov, V., & Troyk, P. R. J. J. o. n. e. (2010). Neuronal loss due to prolonged controlled-current stimulation with chronically implanted microelectrodes in the cat cerebral cortex. *7*(3), 036005.

McCreery, D. B., Agnew, W. F., & Bullara, L. A. (2002). The effects of prolonged intracortical microstimulation on the excitability of pyramidal tract neurons in the cat. *Annals of Biomedical Engineering, 30*(1), 107-119.

McCreery, D. B., Agnew, W. F., Yuen, T. G., & Bullara, L. J. I. T. o. B. E. (1990). Charge density and charge per phase as cofactors in neural injury induced by electrical stimulation. *37*(10), 996-1001.

McCreery, D. B., Yuen, T. G., Agnew, W. F., & Bullara, L. A. (1994). Stimulus parameters affecting tissue injury during microstimulation in the cochlear nucleus of the cat. *Hear Res, 77*(1-2), 105-115.

McCreery, D. B., Yuen, T. G., Agnew, W. F., & Bullara, L. A. (1997). A characterization of the effects on neuronal excitability due to prolonged microstimulation with chronically implanted microelectrodes. *IEEE Transactions on Bio-medical Engineering, 44*(10), 931-939. doi:10.1109/10.634645

McIntyre, C. C., & Grill, W. M. (2002). Extracellular stimulation of central neurons: influence of stimulus waveform and frequency on neuronal output. *Journal of Neurophysiology, 88*(4), 1592-1604.

McIntyre, C. C., Grill, W. M., Sherman, D. L., & Thakor, N. V. (2004). Cellular Effects of Deep Brain Stimulation : Model-Based Analysis of Activation and Inhibition Cellular Effects of Deep Brain Stimulation : Model-Based Analysis of Activation and Inhibition. *Journal of Neurophysiology, 91*, 1457-1469. doi:10.1152/jn.00989.2003

McIntyre, C. C., & Hahn, P. J. (2010). Network perspectives on the mechanisms of deep brain stimulation. *Neurobiology of disease, 38*(3), 329-337.

Merrill, D. R., Bikson, M., & Jefferys, J. G. (2005). Electrical stimulation of excitable tissue: design of efficacious and safe protocols. *Journal of Neuroscience Methods, 141*(2), 171-198. doi:S0165-0270(04)00382-6 [pii]
10.1016/j.jneumeth.2004.10.020

Michelson, N. J., & Kozai, T. D. Y. (2018). Isoflurane and Ketamine Differentially Influence Spontaneous and Evoked Laminar Electrophysiology in Mouse V1. *Journal of neurophysiology*.

Michelson, N. J., Vazquez, A. L., Eles, J. R., Salatino, J. W., Purcell, E. K., Williams, J. J., . . . Kozai, T. D. Y. (2018). Multi-scale, multi-modal analysis uncovers complex relationship at the brain tissue-implant neural interface: New Emphasis on the Biological Interface. *Journal of Neural Engineering, 15*(033001).

Morris, B. J., Feasey, K. J., ten Bruggencate, G., Herz, A., & Hollt, V. (1988). Electrical stimulation in vivo increases the expression of proenkephalin mRNA and decreases the expression of prodynorphin mRNA in rat hippocampal granule cells. *Proceedings of the National Academy of Sciences of the United States of America, 85*(9), 3226-3230.

Mortimer, J. T., Shealy, C. N., & Wheeler, C. (1970). Experimental nondestructive electrical stimulation of the brain and spinal cord. *Journal of Neurosurgery, 32*(5), 553-559. doi:10.3171/jns.1970.32.5.0553

Murasugi, C. M., Salzman, C. D., & Newsome, W. T. (1993). Microstimulation in visual area MT: effects of varying pulse amplitude and frequency. *Journal of Neuroscience, 13*(4), 1719-1729.

Overstreet, C., Klein, J., & Tillery, S. H. (2013). Computational modeling of direct neuronal recruitment during intracortical microstimulation in somatosensory cortex. *Journal of Neural Engineering, 10*(6), 066016.

Penfield, W., & Boldrey, E. (1937). Somatic motor and sensory representation in the cerebral cortex of man as studied by electrical stimulation. *Brain, 60*(4), 389-443.

Prasad, A., Xue, Q. S., Dieme, R., Sankar, V., Mayrand, R. C., Nishida, T., . . . Sanchez, J. C. (2014). Abiotic-biotic characterization of Pt/Ir microelectrode arrays in chronic implants. *Frontiers in neuroengineering, 7*, 2. doi:10.3389/fneng.2014.00002

Pudenz, R. H., Bullara, L. A., Dru, D., & Talalla, A. (1975). Electrical stimulation of the brain. II. Effects on the blood-brain barrier. *Surgical neurology, 4*(2), 265-270.

Ranck, J. B. (1975). WHICH ELEMENTS ARE EXCITED IN ELECTRICAL STIMULATION OF MAMMALIAN CENTRAL NERVOUS SYSTEM: A REVIEW. *Brain Research, 98*, 417-440.

Rattay, F. (1999). THE BASIC MECHANISM FOR THE ELECTRICAL STIMULATION OF THE NERVOUS SYSTEM. *Neuroscience Vol. 89, No. 2, pp. 335-346, 1999*.

Richardson, D. E., & Akil, H. (1977a). Pain reduction by electrical brain stimulation in man. Part 1: Acute administration in periaqueductal and periventricular sites. *J Neurosurg, 47*(2), 178-183. doi:10.3171/jns.1977.47.2.0178

Richardson, D. E., & Akil, H. (1977b). Pain reduction by electrical brain stimulation in man. Part 2: Chronic self-administration in the periventricular gray matter. *J Neurosurg, 47*(2), 184-194. doi:10.3171/jns.1977.47.2.0184

Robert, F., Vicenta, S., Thomas, W., Robert, W., Thomas, H., Robert, G., . . . Nina, G. (2010). Electrical stimulation of the anterior nucleus of thalamus for treatment of refractory epilepsy. *Epilepsia, 51*(5), 899-908. doi:doi:10.1111/j.1528-1167.2010.02536.x

Robinson, D., & Fuchs, A. (1969). Eye movements evoked by stimulation of frontal eye fields. *Journal of Neurophysiology, 32*(5), 637-648.

Salatino, J. W., Ludwig, K. A., Kozai, T. D. Y., & Purcell, E. K. (2017). Glial responses to implanted electrodes in the brain. *Nature BME*.

Sankar, T., Chakravarty, M. M., Bescos, A., Lara, M., Obuchi, T., Laxton, A. W., . . . Lozano, A. M. (2015). Deep Brain Stimulation Influences Brain Structure in Alzheimer's Disease. *Brain Stimul, 8*(3), 645-654. doi:10.1016/j.brs.2014.11.020

Sankar, T., Li, S. X., Obuchi, T., Fasano, A., Cohn, M., Hodaie, M., . . . Lozano, A. M. (2016). Structural brain changes following subthalamic nucleus deep brain stimulation in Parkinson's disease. *Movement disorders : official journal of the Movement Disorder Society, 31*(9), 1423-1425. doi:10.1002/mds.26707

Sato, T. R., Gray, N. W., Mainen, Z. F., & Svoboda, K. (2007). The functional microarchitecture of the mouse barrel cortex. *PLoS Biol, 5*(7), e189.

Sem-Jacobsen, C. (1966). Depth-electrographic observations related to Parkinson's disease. Recording and electrical stimulation in the area around the third ventricle. *Journal of Neurosurgery, 24*(1), Suppl: 388-402.

Sem□Jacobsen, C. (1965). Depth electrographic stimulation and treatment of patients with Parkinson's disease including neurosurgical technique. *Acta Neurologica Scandinavica, 41*(S13), 365-376.

Shannon, R. V. (1992). A model of safe levels for electrical stimulation. *IEEE Trans Biomed Eng, 39*(4), 424-426. doi:10.1109/10.126616

Sharp, A. H., McPherson, P. S., Dawson, T. M., Aoki, C., Campbell, K. P., & Snyder, S. H. (1993). Differential immunohistochemical localization of inositol 1, 4, 5-trisphosphate-and ryanodine-sensitive Ca2+ release channels in rat brain. *Journal of Neuroscience, 13*(7), 3051-3063.

Shepherd, R. K., & Javel, E. (1999). Electrical stimulation of the auditory nerve: II. Effect of stimulus waveshape on single fibre response properties. *Hear Res, 130*(1-2), 171-188.

Sherrington, C. (1910). *The integrative action of the nervous system*: CUP Archive.

Smetters, D., Majewska, A., & Yuste, R. (1999). Detecting action potentials in neuronal populations with calcium imaging. *Methods, 18*(2), 215-221.

Smith, D. (1980). Mechanisms of action potential propagation failure at sites of axon branching in the crayfish. *J. Physiol. (1980), 301, pp. 243-259*.

Spiegel, E. A., Wycis, H. T., Marks, M., & Lee, A. (1947). Stereotaxic apparatus for operations on the human brain. *Science, 106*(2754), 349-350.

Stoney Jr, S., Thompson, W., & Asanuma, H. (1968). Excitation of pyramidal tract cells by intracortical microstimulation: effective extent of stimulating current. *Journal of Neurophysiology, 31*(5), 659-669.

Tehovnik, E. J. (1996). Electrical stimulation of neural tissue to evoke behavioral responses. *65*.

Tolias, A. S., Sultan, F., Augath, M., Oeltermann, A., Tehovnik, E. J., Schiller, P. H., & Logothetis, N. K. (2005). Mapping cortical activity elicited with electrical microstimulation using FMRI in the macaque. *Neuron, 48*(6), 901-911.

Veerakumar, A., Challis, C., Gupta, P., Da, J., Upadhyay, A., Beck, S. G., & Berton, O. (2014). Antidepressant-like effects of cortical deep brain stimulation coincide with pro-neuroplastic adaptations of serotonin systems. *Biological psychiatry, 76*(3), 203-212. doi:10.1016/j.biopsych.2013.12.009

Volta, A. (1800). XVII. On the electricity excited by the mere contact of conducting substances of different kinds. In a letter from Mr. Alexander Volta, FRS Professor of Natural Philosophy in the University of Pavia, to the Rt. Hon. Sir Joseph Banks, Bart. KBPR S. *Philosophical transactions of the Royal Society of London, 90*, 403-431.

Wang, Y., & Manis, P. B. (2008). Short-term synaptic depression and recovery at the mature mammalian endbulb of Held synapse in mice. *Journal of Neurophysiology, 100*(3), 1255-1264.

Wang, Z., Feng, Z., & Wei, X. (2018). Axonal Stimulations With a Higher Frequency Generate More Randomness in Neuronal Firing Rather Than Increase Firing Rates in Rat Hippocampus. *Frontiers in Neuroscience, 12*(783). doi:10.3389/fnins.2018.00783

Wei, X. F., & Grill, W. M. (2009). Analysis of high-perimeter planar electrodes for efficient neural stimulation. *Frontiers in neuroengineering, 2*, 15.

Wellman, S. M., Eles, J. R., Ludwig, K. A., Seymour, J. P., Michelson, N. J., McFadden, W. E., . . . Kozai, T. D. (2018). A Materials Roadmap to Functional Neural Interface Design. *Advanced Functional Materials, 28*(12), 201701269. doi:10.1002/adfm.201701269

Wellman, S. M., & Kozai, T. D. Y. (2017). Understanding the Inflammatory Tissue Reaction to Brain Implants To Improve Neurochemical Sensing Performance. *ACS Chemical Neuroscience*. doi:10.1021/acschemneuro.7b00403

Wellman, S. M., & Kozai, T. D. Y. (2018). In vivo spatiotemporal dynamics of NG2 glia activity caused by neural electrode implantation. *Biomaterials, 164*, 121-133.

White, J. J., & Sillitoe, R. V. (2017). Genetic silencing of olivocerebellar synapses causes dystonia-like behaviour in mice. *Nature communications, 8*, 14912.

Wilks, S. J., Hara, S. A., Ross, E. K., Nicolai, E. N., Pignato, P. A., Cates, A. W., & Ludwig, K. A. (2017). Non-clinical and Pre-clinical Testing to Demonstrate Safety of the Barostim Neo Electrode for Activation of Carotid Baroreceptors in Chronic Human Implants. *Frontiers in neuroscience, 11*, 438. doi:10.3389/fnins.2017.00438

Wu, Y., Levy, R., Ashby, P., Tasker, R., & Dostrovsky, J. (2001). Does stimulation of the GPi control dyskinesia by activating inhibitory axons? *Movement Disorders, 16*(2), 208-216.

Xia, Y., Buja, L. M., Scarpulla, R. C., & McMillin, J. B. (1997). Electrical stimulation of neonatal cardiomyocytes results in the sequential activation of nuclear genes governing mitochondrial proliferation and differentiation. *Proceedings of the National Academy of Sciences of the United States of America, 94*(21), 11399-11404.

Xia, Y., McMillin, J. B., Lewis, A., Moore, M., Zhu, W. G., Williams, R. S., & Kellems, R. E. (2000). Electrical stimulation of neonatal cardiac myocytes activates the NFAT3 and GATA4 pathways and up-regulates the adenylosuccinate synthetase 1 gene. *The Journal of biological chemistry, 275*(3), 1855-1863.

Yuen, T. G., Agnew, W. F., Bullara, L. A., Jacques, S., & McCreery, D. B. (1981). Histological evaluation of neural damage from electrical stimulation: considerations for the selection of parameters for clinical application. *Neurosurgery, 9*(3), 292-299.

Supplemental File: Calcium activation of cortical neurons by continuous electrical stimulation: Frequency-dependence, temporal fidelity and activation density

Nicholas J. Michelson[1,2], James R. Eles[1,3], Alberto L. Vazquez[1,3,4,5,6], Kip A Ludwig[7,8], Takashi DY Kozai[1,3,6,9,10*]

1. Department of Bioengineering, University of Pittsburgh, Pittsburgh, PA 15213, USA
2. Department of Psychiatry, University of British Columbia, Vancouver, BC V6T 1Z3, CA
3. Center for the Neural Basis of Cognition, University of Pittsburgh, Pittsburgh, PA 15213, USA
4. Department of Radiology, University of Pittsburgh, Pittsburgh, PA 15213, USA
5. Department of Neurobiology, University of Pittsburgh, Pittsburgh, PA 15213, USA
6. Center for Neuroscience, University of Pittsburgh, Pittsburgh, PA 15213, USA
7. Department of Biomedical Engineering, University of Wisconsin Madison
8. Department of Neurological Surgery, University of Wisconsin Madison
9. McGowan Institute of Regenerative Medicine, University of Pittsburgh, Pittsburgh, PA 15213, USA
10. NeuroTech Center, University of Pittsburgh Brain Institute, Pittsburgh, PA 15213, USA

Abbreviated title: Spatiotemporal activation by microstimulation

Key words: microstimulation, bioelectric medicine, brain-computer interface, deep brain stimulation, neuroprosthetics

Support: NIH NINDS R01NS094396, R01NS094404, R01NS062019, R01NS089688, and R21 NS108098

***Correspondence:** 208 Center for Biotechnology and Bioengineering; 300 Technology Dr. Pittsburgh, PA 15219 tdk18@pitt.edu

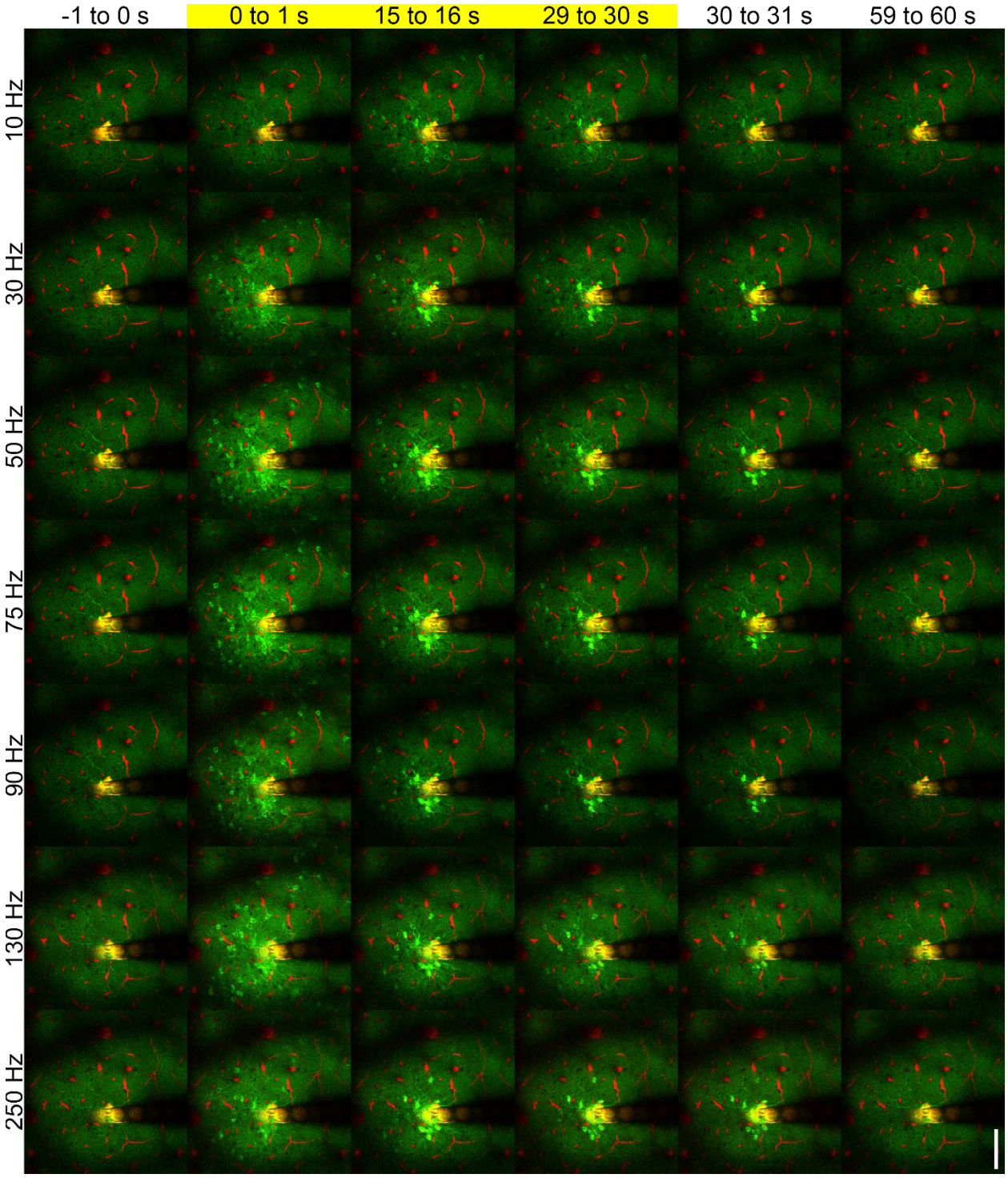

Supplemental Figure 1. Same as figure 3 for all frequencies. Scalebar = 100 µm

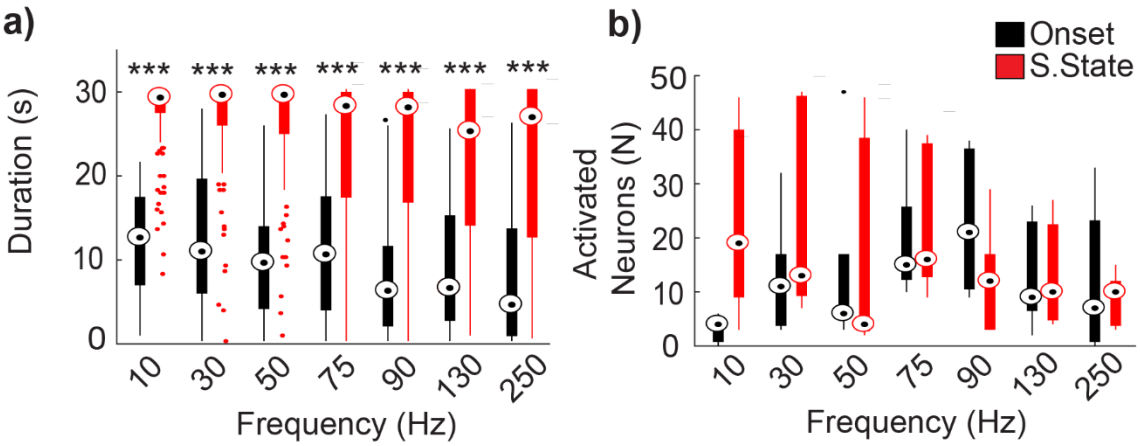

Supplemental Figure 2. (a) Average duration of onset and steady-state phase. Duration of activation phases were calculated by tracking onset-responsive (neurons that are active 0-2s into stimulation) and steady-state-responsive neurons (neurons active 28-30s into stimulation). (b) Average number of neurons activated during onset and steady-state phase for 10Hz, 30Hz, 50Hz, 75Hz, 90Hz, 130Hz and 250 Hz stimulation. For (a): repeated measures two-way (within frequencies, F=374.831, p<0.001) with post-hoc t-tests with Bonferroni correction ***p < 0.001.

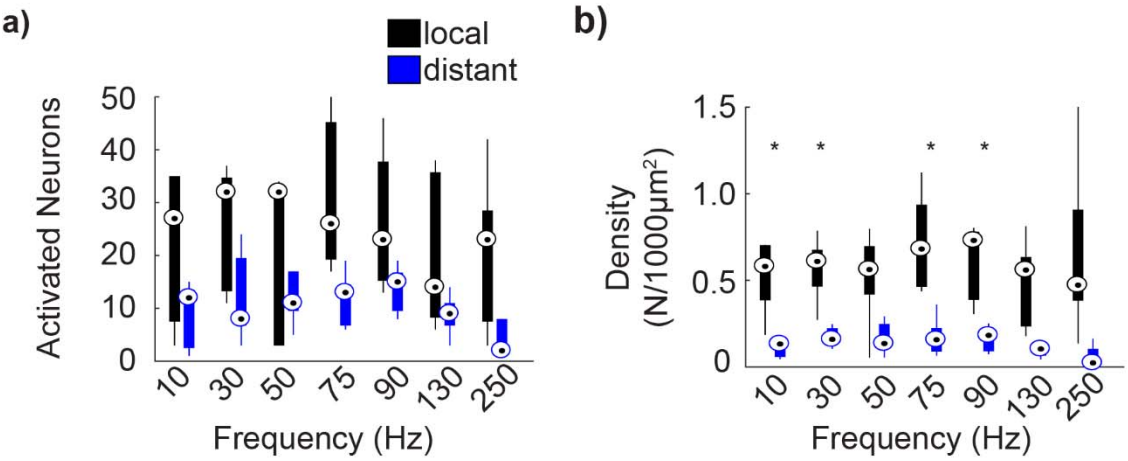

Supplemental Figure 3. (a) Average number of neurons activated that are local and distal from the electrode. (b) Average activation density of local and distal neuron population. Activation density for locally activated neurons was significantly higher for all stimulation frequencies than distally activated neurons. For (b): repeated measures two-way ANOVA (within frequencies, F=523.846, p<0.001) and post-hoc t-tests with Bonferroni correction *p < 0.05

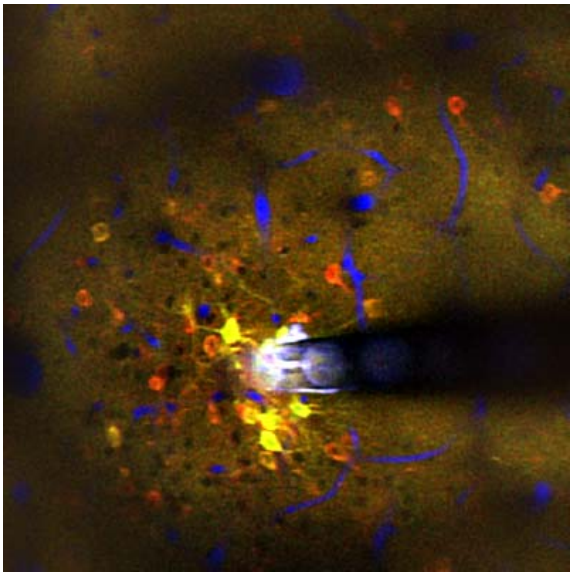

Neuronal microstimulation can treat neurological disorders, but the therapeutic mechanism is not well understood. Microstimulation in mouse cortex produced a spatiotemporal response, activating a sparse population of neurons only at the onset of stimulation (red), and a dense population of neurons throughout the stimulation duration (yellow). Vessels shown in blue.